Implementation of a Wideband Microstrip Phased Array Antenna for X-Band Radar Applications

by

Vernon Pete Davids

Thesis submitted
In partial fulfilment of the requirements for the degree
Magister Technologiae in Electrical Engineering

at the

Cape Peninsula University of Technology

Supervisor:	Co-supervisor:
Prof. Robert van Zyl	Prof. Robert Lehmensiek

Bellville
June 2009

Declaration

I, Vernon Pete Davids, declare that the contents of this thesis represent my own unaided work, and that the thesis has not previously been submitted for academic examination towards any qualification. Furthermore, it represents my own opinions and not necessarily those of the Cape Peninsula University of Technology.

Signed: ..... Date: ....10 July 2009.....

Vernon P. Davids

Abstract

This thesis presents the design, analysis and implementation of an eight-element phased array antenna for wideband X-band applications. The microstrip phased array antenna is designed using eight quasi-Yagi antennas in a linear configuration and is printed on RT/Duroid 6010LM substrate made by Rogers Corporation. The feeding network entails a uniform beamforming network as well as a non-uniform −25 dB Dolph-Tschebyscheff beamforming network, each with and without 45° delay lines, generating a squinted beam 14° from boresight. Antenna parameters such as gain, radiation patterns and impedance bandwidth (BW) are investigated in the single element as well as the array environment. Mutual coupling between the elements in the array is also predicted.

The quasi-Yagi radiator employed as radiating element in the array measured an exceptional impedance bandwidth (BW) of 50% for a $S_{11} < -10$ dB from 6 GHz to 14 GHz, with 3 dB to 5 dB of absolute gain in the frequency range from 8 GHz to 11.5 GHz. The uniform broadside array measured an impedance BW of 20% over the frequency band and a gain between 9 dB to 11 dB, whereas the non-uniform broadside array measured a gain of 9 dB to 11 dB and an impedance BW of 14.5%. Radiation patterns are stable across the X-band. Beam scanning is illustrated in the E-plane for the uniform array as well as for the non-uniform array.

Acknowledgements

I wish to express my sincere words of gratitude to:

- God for his kind blessings.
- Prof. Robert van Zyl (CPUT/F'SATI), for his academic, personal guidance, always encouraging support, for allowing me to pursue a topic which I am passionate about and his help in defining this research.
- Prof. Robert Lehmensiek (EMSS/CPUT), for his specialised support and expertise in modelling, simulating and measurement of the antennas. I would like to thank him for his diligent and detailed approach in all aspects of this research.
- Mr Jacques Roux (ETSE Electronics) and Mr Deon Kallis (CPUT), for their insightful suggestions, technical and practical interactions and intuitive discussions in this exciting field.
- Mr Iegshaan Khan, Denzil & Berenice (Trax interconnect), for their assistance during the manufacturing process.
- Mr M. Siebers (Stellenbosch University) for the professional and meticulous measurements taken, occasionally at short notice.
- Mr Jason Witkowsky for his ever helping attitude and contacts built through him.
- My parents Petrus and Lea Davids for their undying love and dedicated support throughout my life. This work would not be possible without their faith in me. I am grateful to my entire family for their encouraging words.
- The financial assistance of the CPUT postgraduate office and CSIR towards this research.

Dedication

To

my parents

Petrus Davids & *Lea Davids*

Contents

List of figures

List of tables

Glossary

Abbreviations		Definition
AF	=	Array Factor
AWR	=	Applied Wave Research
BW	=	Bandwidth
CAD	=	Computer Aided Design
CATR	=	Compact Antenna Test Range
CEM	=	Computational Electromagnetics
CPS	=	Coplanar Stripline
CPUT	=	Cape Peninsula University of Technology
CPW	=	Co-planar Waveguide
DC	=	Direct Current
EM	=	Electromagnetic
EMSS	=	EM Software and Systems
FEKO	=	3-D EM software suite of EMSS
FNBW	=	First-Null Beamwidth
HPBW	=	Half-Power Beamwidth
MMICs	=	Monolithic Microwave Integrated Circuits
MoM	=	Method of Moments
MWO	=	Microwave Office software suite of AWR
PCB	=	Printed Circuit Board
PEC	=	Perfect Electric Conductor
SEP	=	Surface Equivalence Principle
SLL	=	Sidelobe Level
UP	=	University of Pretoria
US	=	University of Stellenbosch
UWB	=	Ultra-wideband
VEP	=	Volume Equivalence Principle

Chapter 1 : Research study

1.1 Introduction

It has been one hundred and forty five years since James Clerk Maxwell predicted the existence of electromagnetic (EM) waves in a paper presented in 1864 (Rhea, 2008:26-32). The progress made in modern antenna design and manufacturing involves computer aided design (CAD) and cost effective production techniques. Recent trends and developments involve integration of direct current (DC) and microwave circuitry on multilayered substrates. By using planar stripline techniques in phased array radar systems, accurate control of amplitude and phase distribution across the antenna array is possible. By using wideband radiating elements and feeding networks, a wideband phased array antenna can be realised.

The aim of this research is to address the bandwidth (BW) demands within the phased array radar systems we see today. As predicted in conceded research a decade ago we see presently the utilisation of microstrip phased array antennas conforming to the surfaces of vehicles, aircraft, ships, missiles and numerous other platforms. The driving force for this is the requirements for lower-cost, lightweight and low-profile antennas for state of the art antenna systems. CAD techniques have become compulsory in the design, analysis and fabrication of microstrip antennas and arrays. The CAD approach has been utilised extensively where possible as an aid for modelling, analysis and optimisation within this research. Electromagnetic (EM) modelling was performed making extensive use of FEKO (version 5.4) from EM Software and Systems (EMSS). The core of the FEKO program is based on the MoM which is a full wave solution of Maxwell's integral equations in the frequency domain.

1.2 Background

Phased array antennas were realised during the 1960s (Hansen, 1998:1-1). Today, ground- and space-based communication systems require advanced pattern control features as well as the ability to alter transmission and reception patterns for gain and sidelobe optimisation. Modern radar system requirements demand a lightweight, small and conformal antenna. Other, equally important characteristics include cost and ease of manufacture.

Microstrip arrays have been widely researched and published as suitable candidates for phased array antennas. These arrays are attractive at millimeter-wave applications because of their small volume, light weight and controllable scanning using electronic phase control. Earlier microstrip arrays utilised the fundamental square and circular patch antennas as radiating elements. Later advances included fabricating multilayered antenna systems. Mailloux (1980:303-307) discusses the progress made in these earlier phased array technologies. Developments and trends in microstrip antennas and arrays are covered in the work of James, Hall and Wood (1980:309-314). The authors concluded by stating BW and the sidelobe level (SLL) as being the most significant residual problem for military applications.

In radar applications, it is essential to cope with unwanted sidelobe clutter and sidelobe interference. This is accomplished by employing antennas with narrow beams and very low sidelobes. Antennas possessing sidelobes 40 dB below the main lobe peak are said to contain ultra-low sidelobes (Brookner, 1988:19-19). Brookner demonstrates a dipole array antenna achieving ultra-low sidelobes over the frequency band 1.2 GHz to 1.4 GHz. The entire antenna, including radiating elements, as well as feeding network was photo-etched on a honeycomb stripline medium. Brookner also justifies the use of the low dielectric honeycomb substrate since it minimises phase and amplitude errors due to inhomogeneities in the dielectric constant.

Increasing the operational BW is one of the most researched parameters of microstrip antennas due to the introduction of Ultra-Wideband (UWB) applications. Yun, Wang, Zepeda, Rodenbeck, Coutant, Li and Chang (2002:641-650) present a phased array system with full-duplex operation and wide-beam scanning. The authors made use of a wideband power divider, and a stripline-fed Vivaldi antenna array. Vivaldi antennas are renowned for their wide operational BW and are frequently used as radiators in array antennas.

An antenna array utilising a modified printed bow-tie antenna operating from 5.5 GHz to 12.5 GHz is presented by Eldek, Elsherbeni and Smith (2005:939-943). Lai, Liu and Jeng (2006) proposed a cost-effective wideband planar antenna array system for multiple wireless applications. The system can be integrated on a single substrate, thus lowering fabrication cost.

1.3 Addressing the problem

For phased array systems, the antenna element should have wide beamwidth, low mutual coupling and wide BW (Alhalabi & Rebeiz, 2008:3136-3142). Many different techniques have been proposed in an effort to increase the impedance BW of microstrip antennas over the years. The most widely used elements for phased array systems include the patch antenna, dipole antenna, Vivaldi, bow-tie, and the Yagi antenna.

Patch antennas bring forth many previously mentioned advantages but suffer from narrow BWs, however, many authors achieved reasonable success. Rigoland, Drissi, Terret and Gadenne (1996:163-167) demonstrated two wideband planar arrays for radar applications. The authors achieved a BW of 15% to 20% in the C- and X-band for a monopolar array and dual polarised flat array respectively. The arrays displayed good BW and radiation performance. Low sidelobes in the order of –25 dB were achieved through the use of unequal Wilkinson power dividers. Discontinuities at the T-junctions of the power dividers with higher power ratios were optimised using CAD modelling tools. Discontinuities are one of the major problems when designing and implementing microstrip feeding networks.

The dipole antenna is relatively easy to implement on microstrip and many authors claim moderate BWs. Chang, Kim, Hwang, Sim, Yoon and Yoon (2003:346–347) made use of a dipole and parasitic element as a director, with the length of the director made longer than the dipole itself. The effect is a dipole resonant at 2.1 GHz with the director at 1.8 GHz which increases the BW. The antenna displayed a BW of 43%. The antenna is fed by a broadband radial stub balun with a transition which converts the microstrip feeding line into a co-planar stripline (CPS). The dual resonant technique was also utilised by Eldek (2006:1-15) in the design of a double dipole antenna for phased array applications. A simplified balun is used and a BW of more than 84% is reported with good radiation pattern stability over frequency. More innovative research efforts resulted in the design of a high-efficiency angled-dipole antenna by Alhalabi *et al.* (2008:3136-3142). The antenna achieves a gain of 2.5 dB at

20 GHz to 26 GHz and a cross-polarization level of < -15 dB at 24 GHz. The authors made use of a truncated ground plane acting as a reflector. Mutual coupling remained below –23 dB, with an element spacing of 0.5 λ_0 to 0.54 λ_0 from 22 GHz to 24 GHz, where λ_0 is the free space wavelength.

Vivaldi antennas are renowned for their broadband characteristics. However, one of the drawbacks is their occupational size. A large amount of success has been achieved by Beltrán, Chávez, Torres and Garro (2008:267-270) by using Vivaldi antennas as elements in a wideband antenna array. The design utilises four elements fed using 3-dB branch-line couplers and achieves a BW of 50% for a $S_{11} < -10$ dB.

The printed bow-tie antenna is in essence a wideband dipole antenna. A microstrip fed modified printed bow-tie antenna operating in the C- and X-band is illustrated by Eldek *et al.* (2005: 939-943). The authors achieved a 91% impedance BW for a VSWR < 2.

The Yagi-Uda antenna was first published in 1928 and has been extensively researched and used as an end-fire antenna. Regardless of this early realisation, limited success is reported in efforts to adapt this antenna to microwave/millimeter wave applications on planar substrates. Several fascinating and creative approaches arrived with efforts to implement this antenna in microstrip. Kaneda *et al.* (1999) presented for the first time a uniplanar quasi-Yagi antenna printed on a single layer of high dielectric constant substrate (see Figure 1.1 below).

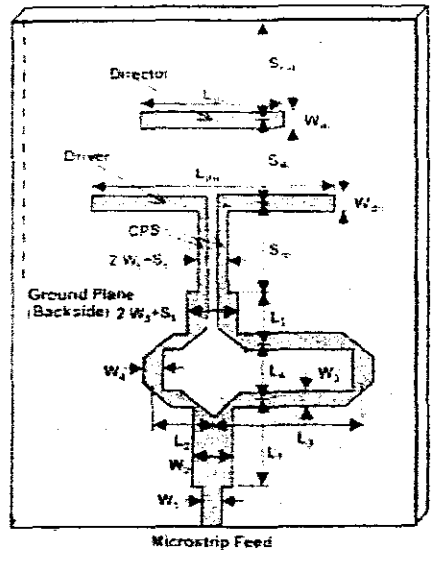

Figure 1.1: Quasi-Yagi antenna (Qian, Deal, Kaneda & Itoh, 1999:911).

The reported performance of the antenna measures a 48% BW for a VSWR < 2, 6.5 dB of gain, an end-fire beam with a front-to-back ratio greater than 15 dB and a cross polarization level below −12 dB across the entire X-band. Mutual coupling is measured below −22 dB for two elements spaced $\lambda_0/2$ at the centre frequency of 10 GHz.

Various other researchers pursued this antenna design with slight modifications, with the intention of optimised gain and BW. Kan, Waterhouse, Abbosh & Bialkowski (2007:18-20) presented a coplanar waveguide (CPW) fed quasi-Yagi antenna with broad BW covering the X-band. The antenna utilised two directors, a driven element and a suspended ground plane acting as a reflector element. The antenna measures a 44% BW for VSWR < 2, front-to-back ratio of 15 dB, efficiency of 95% and a gain of 7.4 dBi. The increased gain is attributed to the addition of an extra director. The quasi-Yagi antenna was also successfully down scaled in frequency and implemented by various other researchers.

A quasi-Yagi antenna is fed with a balun, which provides symmetry and matching of a feeding microstrip line to balanced CPS. Song, Bialkowski and Kabacik (2000:166–169) investigated the dimensional parameters of the quasi-Yagi antenna and the effects of the balun on the input return loss. The effects of the balun on the radiation performance were also studied by García, Casaleiz, Segura, Otero and Peñalosa (2006:320-323).

The array antenna was divided into two design problems identified as the radiating elements and the beamforming network. The beamforming network is further subdivided into power dividers and a phase shifting network as seen in Figure 1.2.

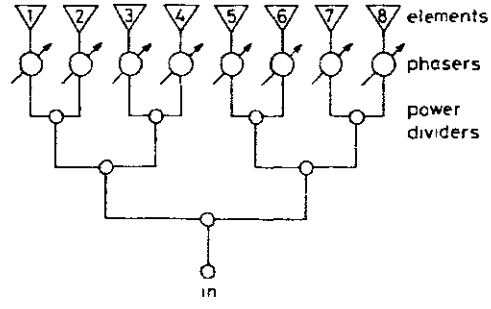

Figure 1.2: Phased array topology (Rudge, Milne, Olver & Knight, (eds). 1983:100)

Due to the favourable radiation performance and impedance BW depicted by the quasi-Yagi antenna it was decided to employ this antenna as the radiating element in an eight-element linear phased array antenna. To ensure power is distributed correctly to all elements and over the entire X-band, a uniform beamforming network using multi-section 3-dB power dividers was developed. To achieve low sidelobes, preferred in radar applications, a Dolph-Tschebyscheff beamforming network is pursued making use of unequal power dividers. The beam of this array was scanned in the E-plane by the addition of a phase delay circuit.

1.4 Objective

The objective of this research entails the development of a phased array antenna constituting a lightweight, low profile and inexpensive design. The antenna should operate at X-band. A requirement for radar applications involves a low sidelobe design as well as narrow beamwidths. Therefore, it is necessary to develop a beamforming network to minimise these sidelobes. Beam scanning in the E-plane is required and a beam steering circuit should be realised, complimenting the array construction. Measured results are compared with theoretical and predicted results.

1.5 Research process

1.5.1 Research problem

There exists a requirement in radar applications to develop a lightweight, cost-effective, low-profile and compact phased array antenna capable of scanning its main beam through the E-plane as with surveillance radar. The other problem under investigation is the operational BW since the advent of wideband radar systems. Further requirements include narrow beamwidths and low SLLs.

1.5.2 Research question

- The evident question at hand would be how to develop a cost effective, lightweight, low profile and compact phased array antenna.

1.5.3 Investigative question

- With BW being a required characteristic in microstrip antennas, a viable technique is needed to ensure wideband operation of the microstrip array and beamforming networks.
- Other requirements of the array antenna are to achieve beam scanning and realise narrow beamwidths as well as low SLLs. To achieve these requirements a suitable beamforming network implemented on microstrip is needed.
- When designing phased array antennas, mutual coupling must be taken into consideration since it can affect the performance of the array adversely. An attempt to predict mutual coupling and its effects is thus necessary.

1.6 Research design and methodology

The research process starts with a comprehensive literature study based on published journal and conference papers, as well as reputable books. To predict the outcome, simulation studies of antenna models and sub-models have been developed. Two feeding networks are developed to investigate SLLs and beamwidths. The first was a uniform beamforming network and the second a non-uniform beamforming network with a –25 dB Dolph-Tschebyscheff amplitude taper. Optimisation was done to ensure the design requirements were met. After optimising the models a manufacturing process follows where the final design is then photo-etched using controlled fabrication processes. The antennas are measured and compared with the predicted results. Conclusions are drawn and recommendations given.

1.7 Delimitation

The number of elements was chosen to be eight, based on simplicity, cost and computational power available and was placed in a linear configuration. Therefore, only topics relating to linear arrays will be handled. The array is passive and no active components are used either for gain or beam scanning purposes. The frequency band under investigation is the X-band and is taken to be 8 GHz to 12 GHz in this research. All circuits are implemented using Rogers 6010LM substrate in a microstrip topology. The radiating element under investigation is a quasi-Yagi based on the work done by Kaneda *et al.* (2000:910-918).

1.8 Overview of chapters and layout

Chapter 1 introduces the research study and involves a brief background. Research conducted and techniques employed in order to satisfy system requirements such as impedance BW and low sidelobes are looked at. A summary of research on antenna elements employed in planar microstrip array antennas are compared. The research process and objectives are discussed.

The quasi-Yagi employed as the radiating element is modelled and analysed in Chapter 2. The simulated and measured S-parameters and far-field patterns are presented.

In Chapter 3 an array of eight quasi-Yagi elements are modelled investigating far-field patterns. Mutual coupling is also examined and the effect of the balun and director element.

Chapter 4 involves the design and simulation of the beamforming networks. A uniform and non-uniform beamforming network is designed. To accomplish beam scanning, a delay line phase shifter is also designed.

The elements and beamforming networks are combined in Chapter 5 to form the wideband microstrip array. The final measurements are compared with predicted measurements and presented in this chapter.

Finally, chapter 6 consists of the findings, concluding remarks and recommendations made.

Chapter 2 : Radiating element

2.1 Introduction

Today, microstrip antennas are often found in applications onboard high-performance aircraft, spacecraft, satellites, missiles, cars and mobile phones. This is due to the many advantages presented by microstrip antennas, which include their low profile and conformity. They are also inexpensive to fabricate using printed-circuit technology, mechanically robust, compatible with monolithic microwave integrated circuits (MMICs) and are very versatile in terms of resonant frequency, polarisation, pattern and impedance. Microstrip antennas come in limitless geometries and sizes. The simplest ones are the square, rectangular, and circular patch as well as the printed dipole. Printed dipoles are attractive for their simplicity, broad BW and small size which are favourable characteristics in array antennas.

2.2 Printed dipoles

Two general approaches exist when implementing planar dipoles. The first is to print the dipole on one side of a dielectric substrate. The second method is by printing each arm on each side of a dielectric substrate and feeding the dipole from the one side of the substrate. The two printed dipole implementations are shown in Figure 2.1.

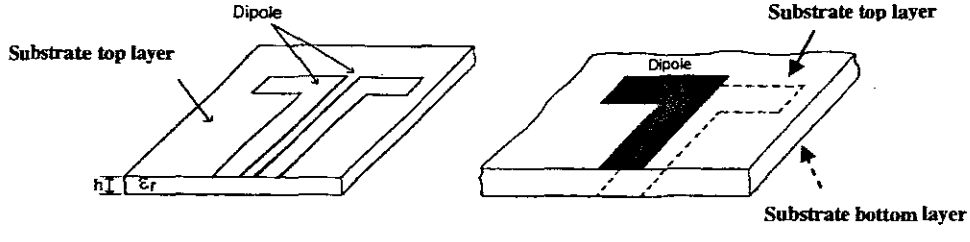

Figure 2.1: Printed dipoles (Garg, Bhartia, Bahl and Ittipiboon, 2001: 400-401).

The most common feeding techniques used for printed dipoles involve the coaxial feed, CPS feed and the coupled-line feed. Figure 2.2 illustrate these types of feeding methods. The CPS feed is the most compatible, physically and electrically with the CPS printed dipole. To feed the planar dipole using other geometries such as microstrip, coplanar waveguide or coaxial probe, a suitable transition to CPS is needed.

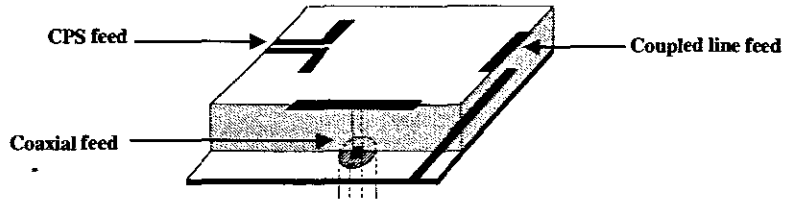

Figure 2.2: Feeding schemes for planar dipoles (Eldek *et al.*, 2005: 940).

Baluns are used when feeding microstrip dipoles and play two major roles, first as a converter from an unbalanced transmission line to a balanced transmission line and secondly as an impedance transformer. Feeding microstrip dipoles involves ingenuity and many authors have utilised different techniques to accomplish a balanced feed for these antennas. Alhalabi *et al.*, (2008:3136-3142) presented a differential angled dipole fed by a single-ended microstrip line. The feed used a truncated ground plane, yielding excellent BW performance from 20 GHz to 26 GHz. An equally successful topology involved a balun which makes the transition between the microstrip line and CPS lines by feeding the dipole with equal magnitude but 180° out of phase (Kaneda *et al.*, 1999:910-918). This is accomplished by making the feed line feeding the one arm $\lambda/2$ longer than the line feeding the other arm, as seen in Figure 1.1. An alternative to this method is to gradually transform the electric field distribution of the microstrip line to that of the CPS by optimally tapering the ground conductor trace to provide impedance as well as field matching. Figure 2.3 illustrates the tapered balun analysed by Woo, Kim, Kim and Cho (2008:2068-2071). Baluns are also printed in CPW as proposed by Kan, Waterhouse, Abbosh & Bialkowski (2007:18-20).

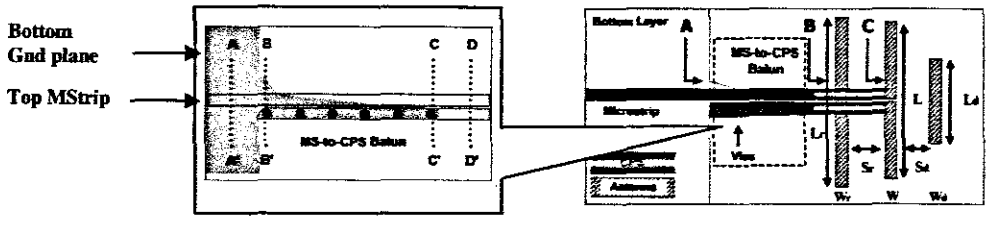

Figure 2.3: Tapered balun (Woo, Kim, Kim, Cho, 2008:2069).

2.3 FEKO model of the quasi-Yagi radiator

The EM model of the quasi-Yagi radiator was constructed in FEKO for analysis. The simulated performance across the X-band was compared with measurements and published data. The antenna is excited with a microstip feed followed by a microstrip balun ensuring a balanced condition for the CPS transition. The CPS feeds the driver dipole and energy is coupled to a printed dipole director. The model is $\lambda_0/2$ by $\lambda_0/2$ (15 mm by 15 mm) at the centre frequency of 10 GHz. The distinctiveness of the design is the truncated ground plane substituting a reflecting element, yielding a compact antenna as seen in Figure 2.4 below.

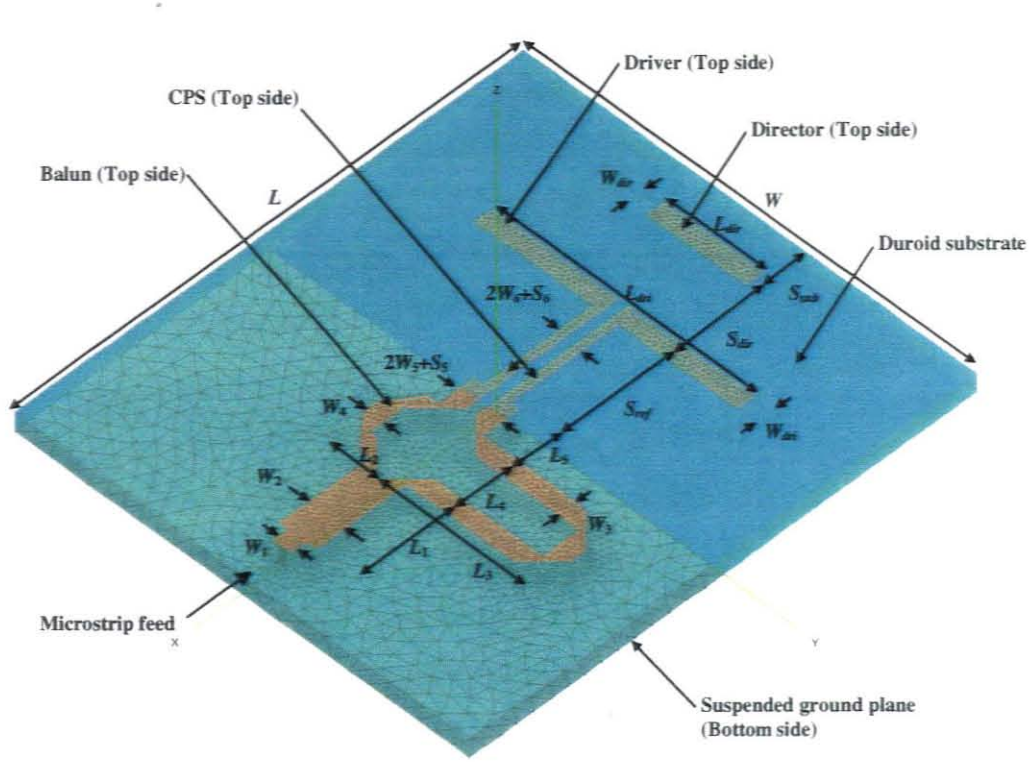

Figure 2.4: 3-D transparent view of the quasi-Yagi antenna model

Table 2.1 and Table 2.2 gives the dimensions as optimised by Kaneda for X-band operation. The characteristic impedance and line lengths were determined with TX-line (2003) and verified with AppCAD (Version 3.0.2) for a Duroid 6010LM substrate, with $\varepsilon_r = 10.2$, $tan\ \delta = 0.0023$, height of $h = 0.635$ mm and copper thickness of $t = 0$ mm. This approximation of the copper thickness is comparable to a thickness of $t = 17$ µm. The distinction between using the approximated copper thickness and actual thickness affects the line lengths and widths by 0.01 λ_g and 0.01 mm, respectively, where λ_g is the guide wavelength.

Table 2.1: Quasi-Yagi dimensions and impedance values

Dimensions Line widths [mm]	Characteristic Impedance [Ohm]
$W_1 = W_3 = W_4 = W_5 = W_{dri} = W_{dir} = 0.5$ mm	50.18
$W_2 = 1.2$ mm	34.48
$W_6 = S_5 = S_6 = 0.3$ mm	67.20

Table 2.2: Quasi-Yagi dimensions and line lengths

Dimensions Line lengths [mm]	Lengths [lambda & Deg]
$L_1 = 3.3$ mm	0.295 λ_g (106°)
$L_2 = L_5 = 1.5$ mm	0.139 λ_g (50.2°)
$L_3 = 4.8$ mm	0.429 λ_g (154.3°)
$L_4 = 1.8$ mm	0.161 λ_g (57.9°)
$S_{ref} = 3.9$ mm	0.348 λ_g (125.4°)
$S_{dir} = 3$ mm	0.268 λ_g (96.4°)
$S_{sub} = 1.5$ mm	0.134 λ_g (48.2°)
$L_{dri} = 8.7$ mm	0.777 λ_g (279.7°)
$L_{dir} = 3.3$ mm	0.295 λ_g (106.1°)
$\lambda_g = 11.2$ mm	1 λ_g (360°)

The surface equivalence principle (SEP) method was used to model the dielectric medium of the antenna. Through experimentation it was found that the SEP converged better for the same segmentation properties than when using the volume equivalence principle (VEP). The VEP also has many more unknowns, and is therefore more memory intensive (FEKO, 2008 (a)). In FEKO feeding is not allowed on the surface of the dielectric. FEKO suggests two options of feeding microstrip lines on finite substrates. The first is to feed the line outside the boundary of the substrate in free-space as seen in Figure 2.5 (a). The second method involves the construction of the feed inside the substrate boundary, as shown in Figure 2.5 (b). It is necessary to feed the line at least one substrate height or greater away from the dielectric wall. Decreasing the width of the feeding edge to approximately $\lambda_0 / 20$ to $\lambda_0 / 30$ may be necessary,

since higher order modes could degrade the impedance match as the frequency increases (FEKO, n.d. 2008 (b)). The feed arrangement in Figure 2.5 (b) was used.

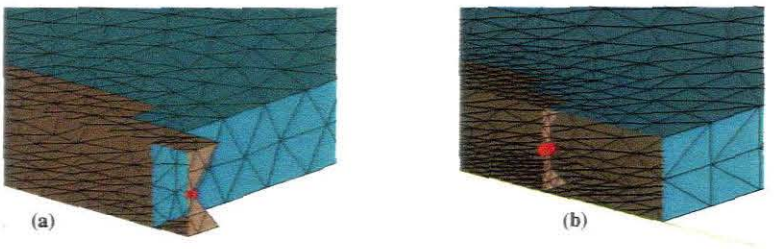

Figure 2.5: Feeding techniques for finite substrates (a) Feeding outside substrate (b) Feeding inside substrate

The model was meshed with an optimum triangle edge length obtained through finding the edge length for which the solution converged. To give an accurate representation of the geometry and surface charge distribution, it was necessary to mesh some parts of the model which had complex geometries finer, especially those parts with metallic triangles. Efficient use of symmetry is very important when CAD modelling is employed since it can dramatically accelerate and reduce the computational time and memory requirements respectively. Symmetry was used extensively where suitable. The quasi-Yagi radiator in Figure 2.4 amounts to 14576 triangles and 43668 unknowns. The simulation was done on a cluster compromising of six computers running six Intel dual core CPUs, with a 64-bit version of LINUX. The model size amounts to 27.6 GBytes and simulated for 15.4 hours.

2.4 Quasi-Yagi radiator results

Three antenna models were constructed, each on a dielectric substrate measuring 15 mm by 15 mm. These models are a planar dipole with suspended ground plane (see Figure 2.6 (a)), a planar dipole with a director and suspended ground plane (quasi-Yagi without balun), (see Figure 2.6 (b)) and a quasi-Yagi with balun (see Figure 2.6 (c)).

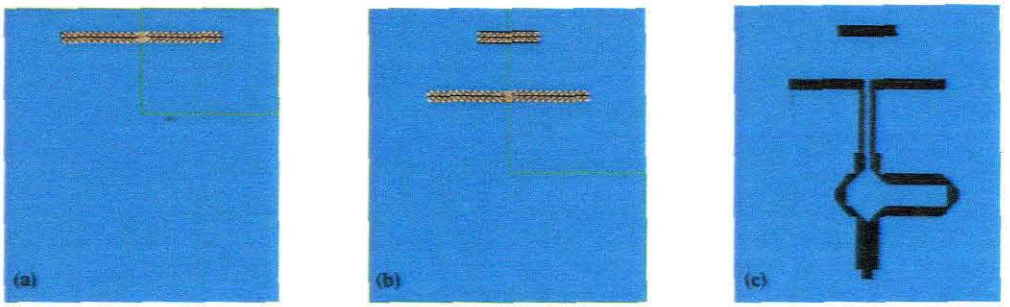

Figure 2.6: Quasi-Yagi models (a) Planar dipole (b) Quasi-Yagi without balun (c) Quasi-Yagi with balun.

The quasi-Yagi radiator with balun was fabricated and measured. The measurement setup is explained in more detail in Chapter 5. The simulated and measured S_{11} for the quasi-Yagi radiator with balun is shown in Figure 2.7. It should be said that the simulated results involve the feeding of the structures using an optimised edge feed inside FEKO compared with the measured results which include the SMA connector mismatch at the transition from coaxial cable to microstrip.

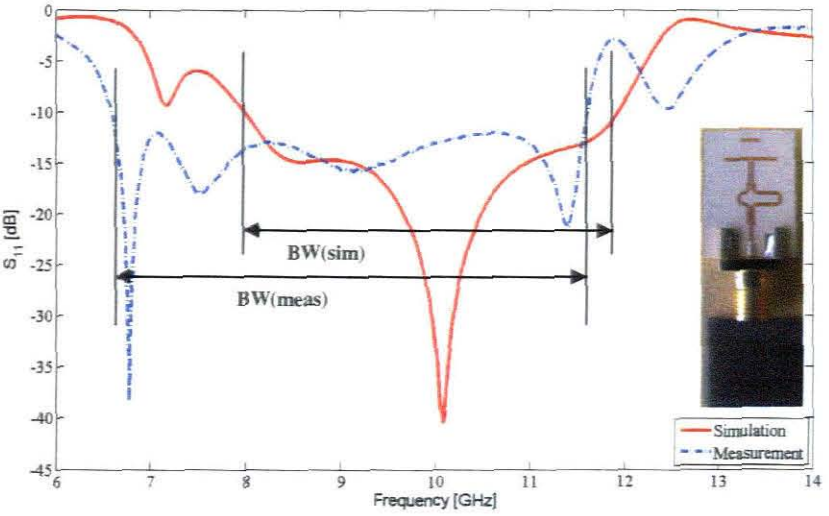

Figure 2.7: $|S_{11}|$ for quasi-Yagi radiator

Based on the researched papers, the measured quasi-Yagi radiator is better matched lower in frequency than the simulated antenna as seen in the research done by Kaneda *et al.* (2000:910-918), Song, Bialkowski and Kabacik (2000:166-169) and Weinmann (2005: 539-542). Figure 2.8 shows the simulated and measured input reflection loss as published by Kaneda *et al.*

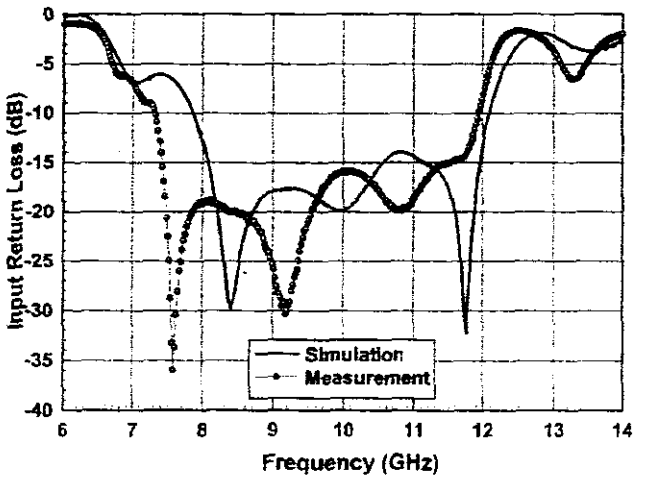

Figure 2.8: Published $|S_{11}|$ for quasi-Yagi radiator (Kaneda *et al.* 1999:911).

The BW is determined relative to the centre frequency as a percentage given by

$$BW = \frac{(f_U - f_L)}{f_0} \times 100\%, \tag{2-1}$$

where f_U and f_L are the upper and lower frequency limits where the input reflection loss amounts to $S_{11} = -10$ dB. The centre frequency is given as

$$f_0 = \frac{1}{2}(f_U + f_L), \tag{2-2}$$

The quasi-Yagi radiator displayed a simulated BW of 40% and measured a significant BW of 50% as illustrated in Figure 2.6. The discrepancies seen in the input reflection loss is similar to those experienced by Kaneda in Figure 2.7.

A parameter study of the quasi-Yagi radiator was carried out by Song (2000: 166-169) using the MoM to analyse the BW performance. The study was done since the quasi-Yagi's design strategy has not been, and is still not, well documented. The conclusions drawn are the following, based on the five design parameters in Figure 2.4 given below:

- Director length (L_{dir})
- Distance between director to driver (S_{dir})
- Gap distance between the CPS (S_6)
- Length of driver (L_{dri})
- Distance between driver to reflector (S_{ref})

The impedance BW is insensitive to changes in the director length and distance between director to driver. The gap between the CPS, if reduced, degrades the return loss moderately. The length of the driver and distance from the reflector are, in contrast, two very sensitive parameters since they affect the impedance BW and design frequency. To shift the impedance BW of the quasi-Yagi radiator to cover the higher frequency range, it is thus necessary to shorten the driver or reduce the distance of the driver from the reflector or both. Apart from being better matched lower in frequency the results show reasonable agreement between simulated, measured and published results. The discrepancy seen in Figure 2.7 is due to the discontinuity caused by the SMA coax to microstrip transition.

The measured gain illustrates a minimum gain of 3.2 dB across the band (see Figure 2.9). The gain agrees well with the reported gain of 3 dB to 5 dB by Kaneda. The simulated gain for the quasi-Yagi radiator, with balun, at 8 GHz, 10 GHz and 11.5 GHz are 5 dB, 3.9 dB and 4 dB respectively. The measured gain ranges from 4.2 dB, 3.6 dB and 4.7 dB corresponding to the gain at 8 GHz, 10 GHz and 11.5 GHz.

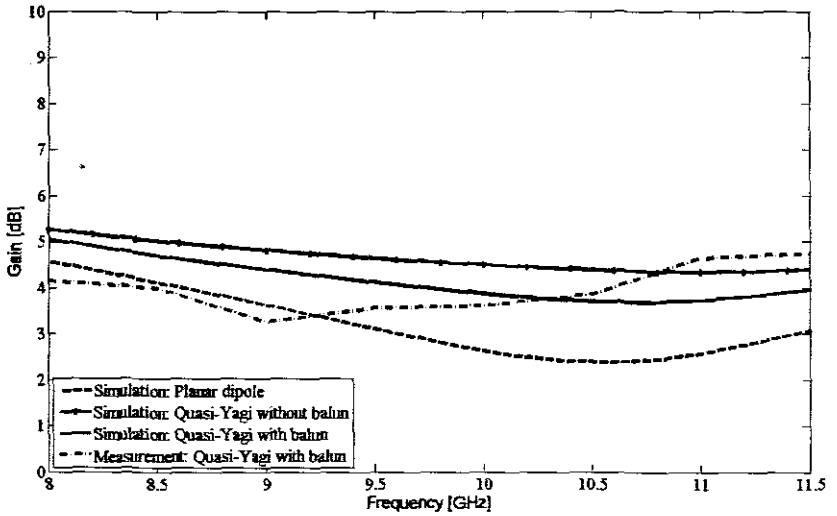

Figure 2.9: Gains for quasi-Yagi radiator

Figure 2.9 shows that the simulated gain result for the planar dipole is the lowest of all three models. This is due to the absence of the director element. The simulated result for the quasi-Yagi radiator without balun displayed the highest gain of all models. The last model is the quasi-Yagi radiator with a microstrip balun and is excited via a microstrip port. This model displayed higher gain than the planar dipole but less than the quasi-Yagi without balun. This can be ascribed to the dielectric, conductor loss and spurious radiation inherent to the microstrip feeding structure of the quasi-Yagi radiator. The planar dipole at 8 GHz, 10 GHz and 11.5 GHz displayed a simulated gain of 4.6 dB, 2.6 dB and 3 dB respectively. The simulated quasi-Yagi radiator without balun showed a gain of 5.3 dB, 4.5 dB and 4.4 dB at 8 GHz, 10 GHz and 11.5 GHz, corresponding to the low, centre and high frequency points of the X-band respectively.

The radiation patterns are simulated across the entire X-band and the E- and H-planes are shown in Figure 2.10 and Figure 2.11 respectively. The E- and H-planes are presented at 8 GHz to 11.5 GHz in steps of 0.5 GHz through the X-band.

The measured gain illustrates a minimum gain of 3.2 dB across the band (see Figure 2.9). The gain agrees well with the reported gain of 3 dB to 5 dB by Kaneda. The simulated gain for the quasi-Yagi radiator, with balun, at 8 GHz, 10 GHz and 11.5 GHz are 5 dB, 3.9 dB and 4 dB respectively. The measured gain ranges from 4.2 dB, 3.6 dB and 4.7 dB corresponding to the gain at 8 GHz, 10 GHz and 11.5 GHz.

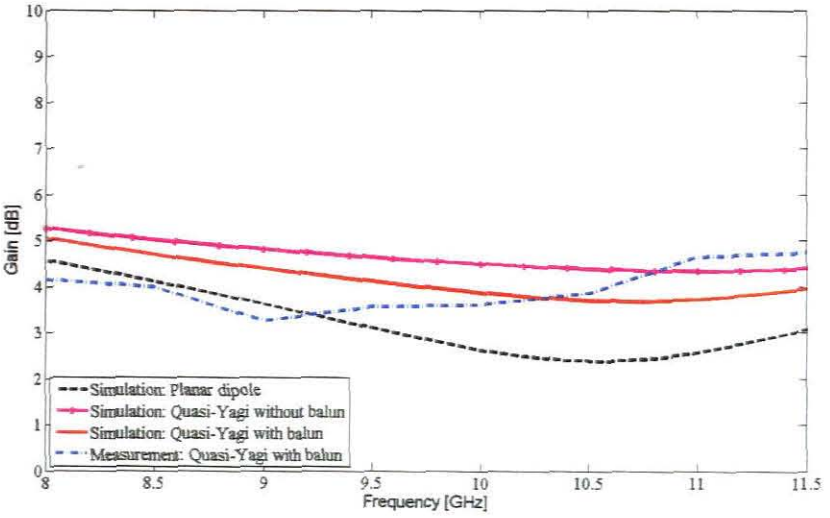

Figure 2.9: Gains for quasi-Yagi radiator

Figure 2.9 shows that the simulated gain result for the planar dipole is the lowest of all three models. This is due to the absence of the director element. The simulated result for the quasi-Yagi radiator without balun displayed the highest gain of all models. The last model is the quasi-Yagi radiator with a microstrip balun and is excited via a microstrip port. This model displayed higher gain than the planar dipole but less than the quasi-Yagi without balun. This can be ascribed to the dielectric, conductor loss and spurious radiation inherent to the microstrip feeding structure of the quasi-Yagi radiator. The planar dipole at 8 GHz, 10 GHz and 11.5 GHz displayed a simulated gain of 4.6 dB, 2.6 dB and 3 dB respectively. The simulated quasi-Yagi radiator without balun showed a gain of 5.3 dB, 4.5 dB and 4.4 dB at 8 GHz, 10 GHz and 11.5 GHz, corresponding to the low, centre and high frequency points of the X-band respectively.

The radiation patterns are simulated across the entire X-band and the E- and H-planes are shown in Figure 2.10 and Figure 2.11 respectively. The E- and H-planes are presented at 8 GHz to 11.5 GHz in steps of 0.5 GHz through the X-band.

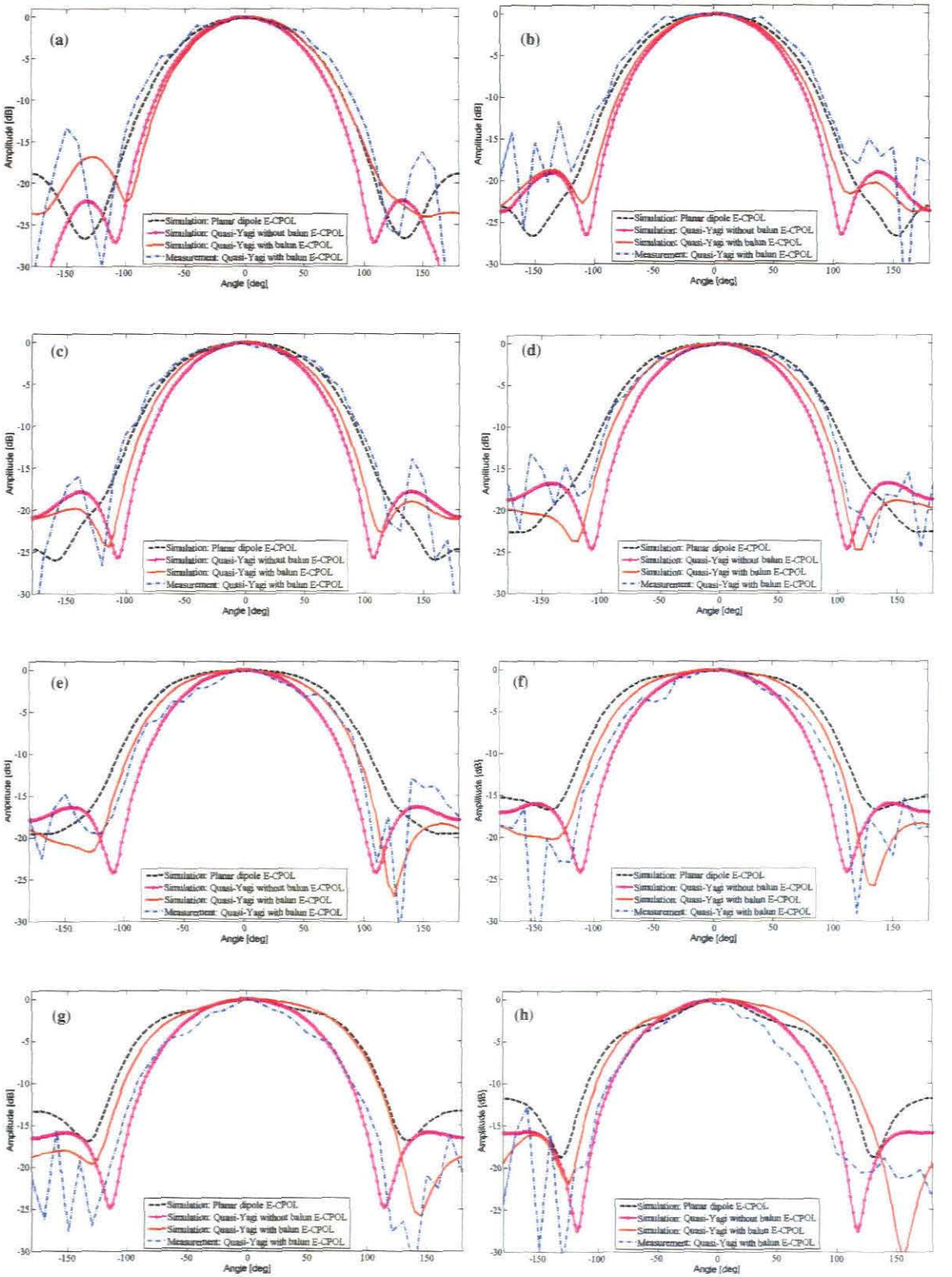

Figure 2.10: E-plane for quasi-Yagi radiator

(a) 8 GHz, (b) 8.5 GHz, (c) 9 GHz, (d) 9.5 GHz, (e) 10 GHz, (f) 10.5 GHz, (g) 11 GHz, (h) 11.5 GHz.

Figure 2.10 shows well-defined end-fire radiation patterns displayed by the quasi-Yagi radiator with a simulated front-to-back ratio better than 18 dB and a measured front-to-back ratio better than 12 dB. The quasi-Yagi radiator yields a simulated HPBW at 8 GHz, 10 GHz and 11.5 GHz amounts to 92°, 126° and 140°, where the measured HPBW corresponds to 107°, 106° and 83° respectively. The difference between the simulation and measurement is believed to be due to measurement errors as well as the SMA coax to microstrip transition.

An H-plane cut is also presented in Figure 2.11 below. Looking at Figure 2.10 and Figure 2.11 it is noticed that the measured radiation patterns do not correlate and amplitude ripples are present, most probably due to the measurement setup and reflections within the test range.

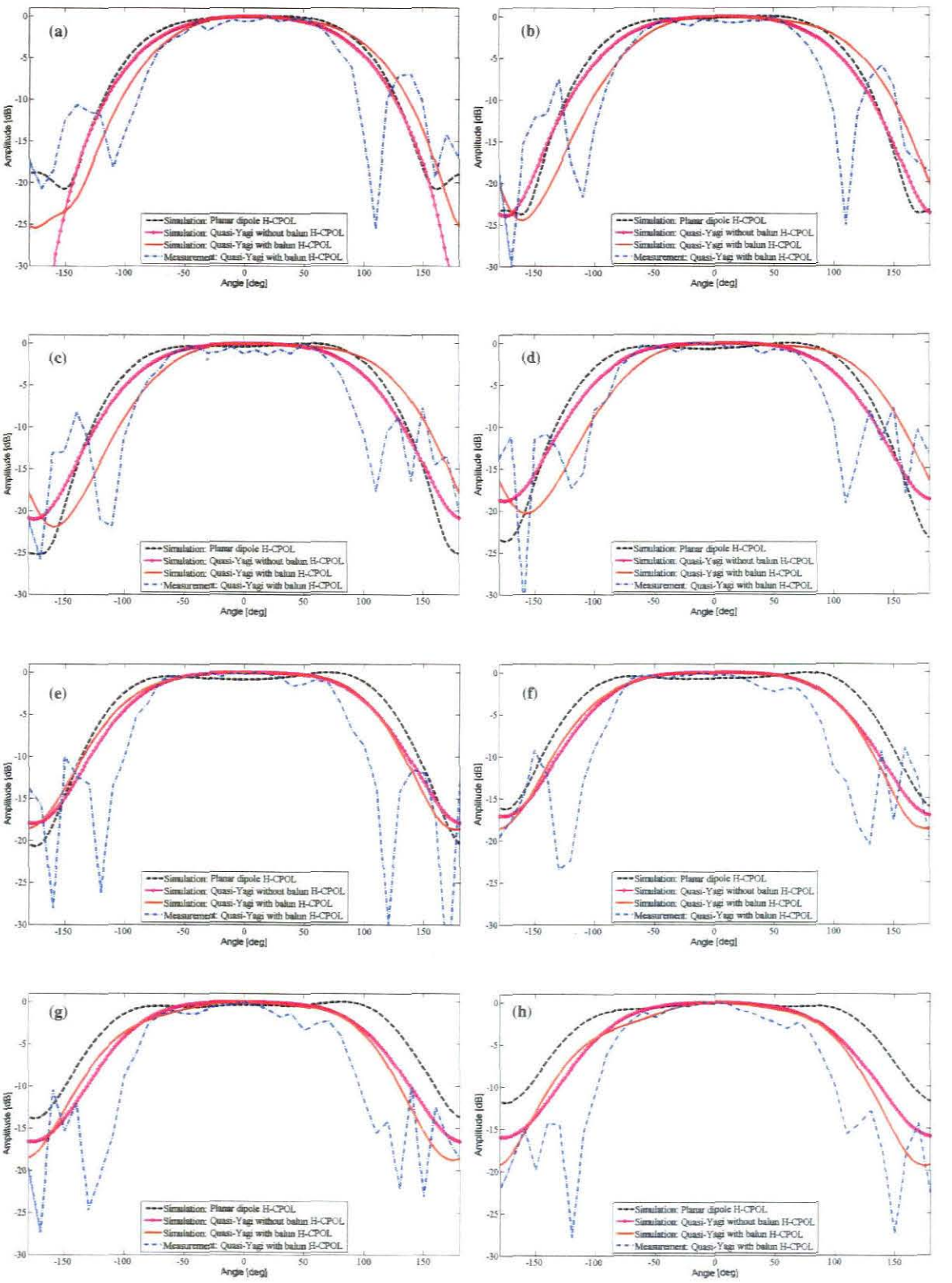

Figure 2.11: H-plane for quasi-Yagi radiator

(a) 8 GHz, (b) 8.5 GHz, (c) 9 GHz, (d) 9.5 GHz, (e) 10 GHz, (f) 10.5 GHz, (g) 11 GHz, (h) 11.5 GHz.

2.5 Summary

In this chapter, the quasi-Yagi radiating element was modelled in FEKO and fabricated. The results of a planar dipole, a quasi-Yagi radiator without balun and a quasi-Yagi radiator with balun were compared. The measured results show good agreement with the simulated results. The performance of the quasi-Yagi radiator makes this antenna an appropriate candidate for phased array antenna designs.

Chapter 3 : Quasi-Yagi array

3.1 Introduction

The radiating characteristics of a single antenna are not adequate for many applications since it either does not supply high enough values of gain, or the radiation pattern geometry does not fulfil the requirement. To increase the gain, the dimensions of the single element can be enlarged, which directly impacts on the manufacturing cost and mechanical constraints associated with a bigger structure. The other option for increasing the gain is by forming an array of radiating elements in an electrical and geometrical configuration. Radiating elements are often chosen to be identical for simplicity, practicality and convenience. Eight quasi-Yagi radiators are modelled in a linear array topology in FEKO and analysed to investigate the radiation performance, gain and mutual coupling.

3.2 FEKO model of quasi-Yagi array

The single quasi-Yagi radiating element is translated to form an array of $N = 8$ elements. These models are constructed to investigate the mutual coupling between elements, the active S_{11} as well as the radiation performance of an array of quasi-Yagi antennas. The element spacing was fixed at $d = 15$ mm corresponding to $\lambda_0/2$ at the centre frequency. Figure 3.1 shows the front and back of the modelled quasi-Yagi array. All elements in the array are excited, initially with uniform amplitude and phase, and later in this thesis, non-uniform amplitude and phase excitations are introduced to investigate lower SLLs as well as beam scanning. The numbering topology used is to label the first element on the far left of the array as element number 1. The element on the far right is thus labelled element number 8 with reference to Figure 3.1. The top view of the quasi-Yagi array with 3-D far-field pattern at 10 GHz, fed with uniform amplitude and phase, is shown in Figure 3.2.

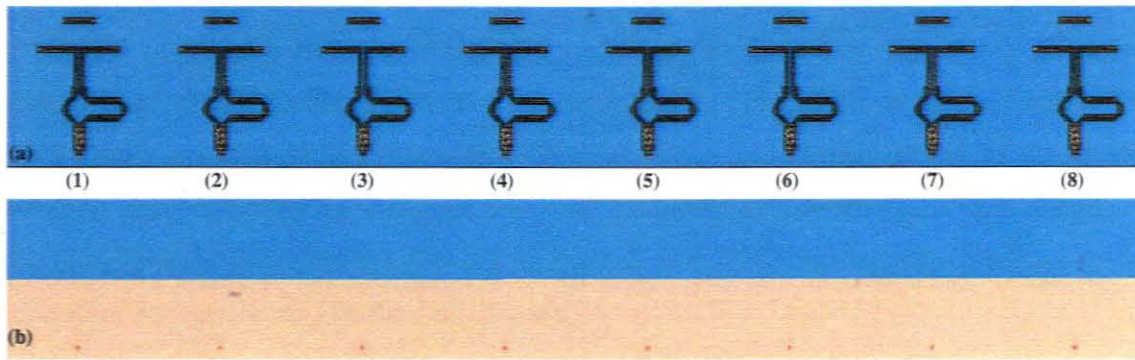

Figure 3.1: Quasi-Yagi array (a) Front of model (b) Back of model

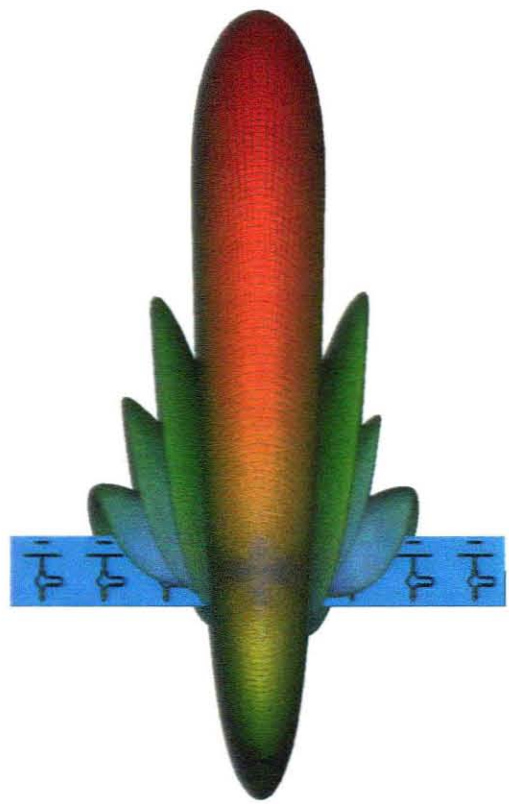

Figure 3.2: Top view of the quasi-Yagi array model with simulated far-field pattern at 10 GHz

3.3 Mutual coupling

In phased array antennas, the element's input impedance is not constant, but varies as a function of scan angle. This effect leads to a mismatch and power is consequently reflected back into the feeding network. Spurious radiation lobes may also develop. There exist conditions where an array antenna is well matched at broadside, but mismatched at certain scan angles, thus degrading radiation at these angles. In phased array antennas, this phenomenon is known as scan blindness. This impedance mismatch is caused by the mutual coupling between radiating elements in close proximity to one another. The amount of coupling between two elements depends on the radiation characteristics of each, the relative separation between them, and their orientation.

Many researchers have calculated mutual coupling between dipoles in an array. Typically, dipoles are arranged in either parallel or collinear configurations when utilised in arrays. Figure 3.1 is an example of the collinear configuration employed in this thesis. Research concludes that mutual coupling for the collinear configuration is due primarily to the TM surface wave launched in the end-fire direction (Garg *et al.*, 2001:425).

The mutual coupling between elements was simulated and is illustrated in Figure 3.3. Subsequently S_{41}, S_{42}, S_{43}, S_{45}, S_{46}, S_{47} and S_{48} were simulated. All powers coupled to the centre two elements are displayed in Figure 3.3. In an effort to investigate possible contributors of mutual coupling, the planar dipole, quasi-Yagi radiator without baluns and quasi-Yagi radiator with baluns were compared as radiating elements in the array. It was envisaged that the coupling for the quasi-Yagi radiator would be less then the planar dipole. This is due to the director element directing energy towards the end-fire direction. This is however not the case as seen in Figure 3.3. The simulated coupling between element four and all other elements remained well below −15 dB for the planar dipole antennas and quasi-Yagi antennas without baluns, shown in Figure 3.3 (a)-(b) respectively. The coupling for the quasi-Yagi antennas with baluns remained below −15 dB over the majority of the frequency band as seen in Figure 3.3 (c). The mutual coupling as measured by Kaneda *et al.* (2000:910-918) remained below −18 dB for the same element spacing of $\lambda_0/2 = 15$ mm. Due to time constrains the mutual coupling between elements could not be measured.

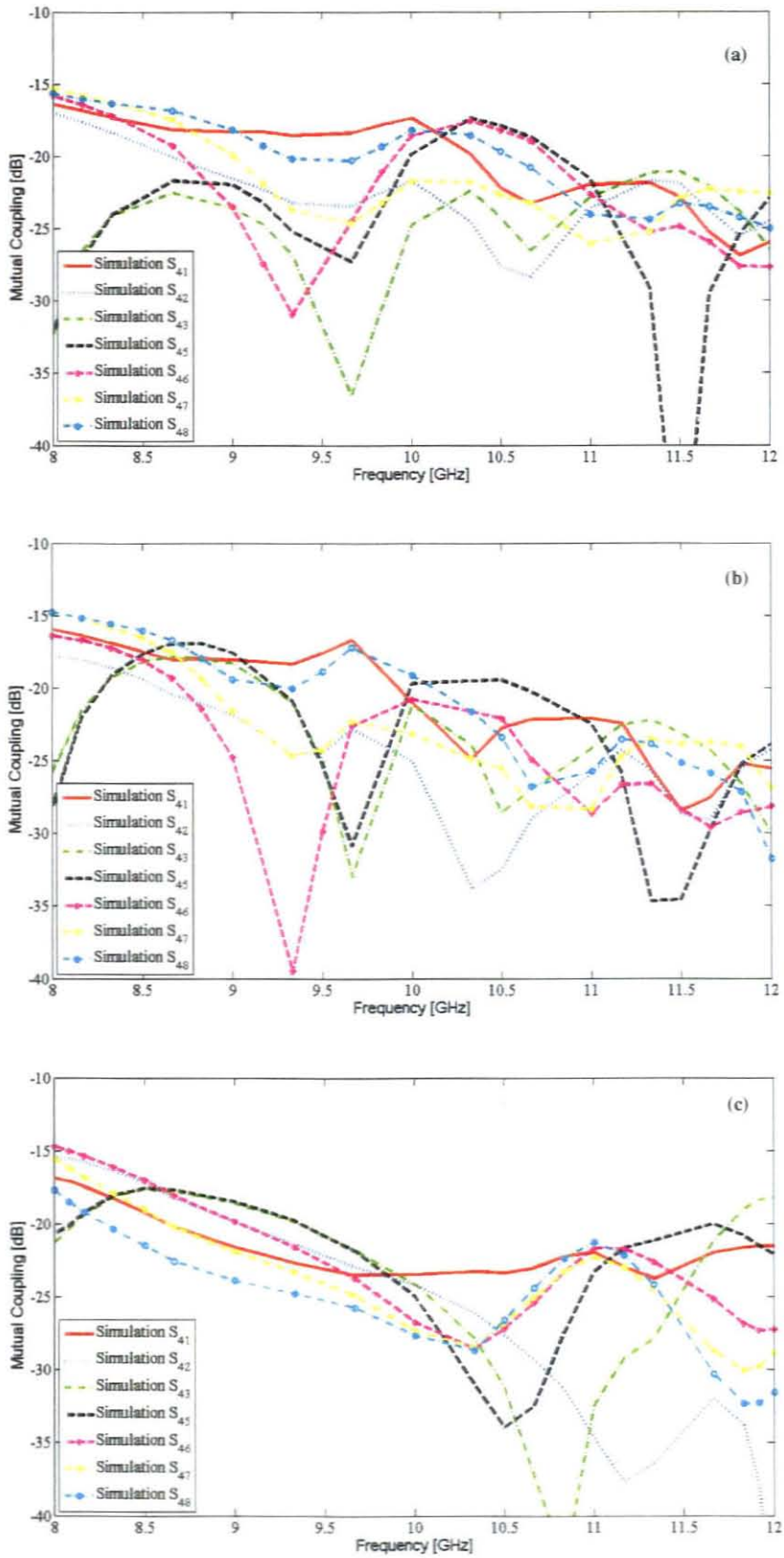

Figure 3.3: Simulated mutual coupling (a) Planar dipole array (b) Quasi-Yagi array without baluns (c) Quasi-Yagi array with baluns

3.4 Quasi-Yagi array results

The radiation performance can be predicted for an $N = 8$ element array with uniform or non-uniform amplitude and phase by using the array theory presented in the subsequent chapter as well as in Appendix A. Figure 3.4 shows the simulated principle E-plane radiation patterns presented at 8 GHz, 10 GHz and 11.5 GHz. Maximum radiation occurs broadside to the axis of the array, as expected for this type of array. The radiation pattern of the uniform array remains stable across the band and the first SLL remains below the theoretical −13.46 dB level, with the exception of the pattern at 8 GHz where the first sidelobe is approximately −9 dB below the main beam as seen in Figure 3.4 (a). Three models are once more compared. These are an array with planar dipoles, an array with quasi-Yagi radiators and the full quasi-Yagi radiators with baluns, as in seen Figure 3.1. The simulated HPBW for the array with quasi-Yagi elements with baluns at 8 GHz, 10 GHz and 11.5 GHz corresponds 15.4°, 12.7° and 11.4° where the measured HPBW corresponds to 15.3°, 12.2° and 10.7° respectively. The simulated HPBW agrees with the measured HPBW. However, it should be understood that the simulated results do not include a beamforming network, and each element is excited with an ideal microstrip port and source. The discrepancies observed in the sidelobes of the simulated and measured results are due to the added uniform beamforming network of the measured array.

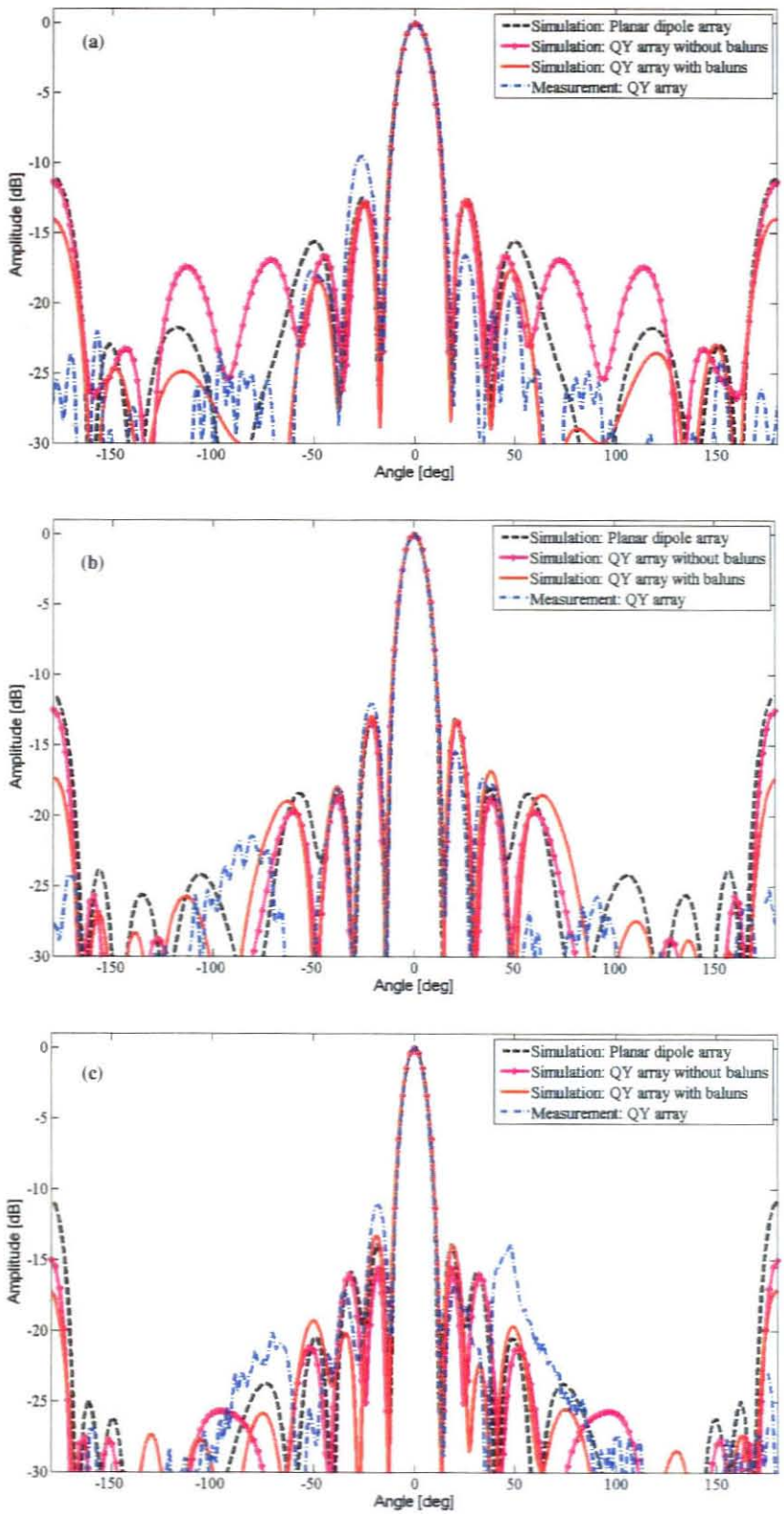

Figure 3.4: E-plane for quasi-Yagi array (a) 8 GHz (b) 10 GHz (c) 11.5 GHz

3.5 Summary

In this chapter the quasi-Yaqi radiator was modelled in an array environment. Mutual coupling was simulated between elements in the eight element linear array. The simulated mutual coupling remained well below −15 dB. Mutual coupling was not measured due to time constraints. The measured coupling reported by Kaneda *et al.* (2000:910-918) remained below −18 dB for the same element spacing of $\lambda_0/2 = 15$ mm. The far-field patterns were also presented at 8 GHz, 10 GHz and 11.5 GHz corresponding to the lower frequency, middle frequency and upper frequency limits of the X-band.

Chapter 4 : Beamforming networks

4.1 Introduction

This section discusses the beamforming networks, which control the distribution of energy across the elements of the array as well as the excitation phase of the feeding currents feeding the individual elements. The radiation characteristics of the array are determined once the aperture distribution is known. The reader is referred to Appendix A for a detailed background of array theory and characteristics of array antennas. The amplitude of the current feeding the radiators is determined through controlling the impedance values of the microstrip feed lines. The phase is altered by introducing a phase delay circuit. Two freeware packages were used to determine the characteristics of the microstrip lines, namely TX-line (2003) from Applied Wave Research (AWR) and AppCAD (Version 3.0.2) from Agilent Technologies. Two beamforming networks are designed, namely a uniform beamforming network and a non-uniform beamforming network. The amplitude and phase distribution at each element in the array are determined based on the radiation requirements, which are a narrow beam directed at boresight, low sidelobes and also to squint the beam from boresight.

4.2 Uniform beamforming network

The first array requirement is an array with a beam directed towards broadside. The theory behind such an array is based on the array theory of an N-element linear array with uniform amplitude and phase discussed in A. 1.2. The elements in the array are placed in a straight line known as a linear configuration. The maximum radiation of the quasi-Yagi element is toward end-fire (see Figure 2.10) and, when configured collinearly in a linear array, maximum radiation is towards broadside ($\theta_0 = 90°$) normal to the axis of the array (see Figure 3.2). To constitute a broadside array, the maximum of the array factor (AF) of the array also needs to be directed toward $\theta_0 = 90°$. The AF for a uniform array with N-elements taking the physical centre of the array as the reference point can be written as

$$AF = \left[\frac{\sin(\frac{N}{2}\psi)}{\sin(\frac{1}{2}\psi)} \right] \tag{4-1}$$

and

$$\psi = kd\cos\theta + \beta, \tag{4-2}$$

where ψ is the progressive phase across the aperture of the array, β is the excitation phase, d is the separation distance, k is the wave number and θ_0 the observation angle.

The AF is a function of the geometry of an array and excitation phase. The excitation phase between the elements of the array β can be calculated by inserting $d = \lambda_0/2$ and $\theta = \theta_0 = 90°$ in equation (4-2). Thus for a beam directed broadside ($\theta_0 = 90°$), equation (4-2) gives the progressive phase as $\psi = 0°$. This denotes that all elements are fed with equal amplitude and equal phase. The element spacing of $d = \lambda_0/2$ is sufficient not to form unwanted grating lobes. The radiation characteristics of the array were numerically computed using MATLAB with the characteristics and outputs summarised in Table 4.1 and Table 4.2 respectively.

Table 4.1: Input characteristics for uniform beamforming network

Input specifications:	
Configuration:	Linear array
Type of array:	Uniform
Radiation pattern:	Broadside (max along $\theta = 90°$)
Number of elements:	$N = 8$
Element spacing:	0.5λ

Table 4.2: Output characteristics for uniform beamforming network

Output of program	
AF Directivity:	9.0309 dB or 8 dimensionless
AF number of maxima between $\theta = 0 - 180°$	= 1
AF $\theta_{(max)}$	$\theta = 90°$
AF HPBW	12.8°
AF SLL	−13.46 dB
Excitation coefficients	$a_1 = 1$ $a_2 = 1$ $a_3 = 1$ $a_4 = 1$

A corporate feed was the apparent choice of feeding the array of elements. The corporate feed has a single input port with eight output ports. Two-way equal power dividers were used to ensure equal amplitude across the array aperture. Figure 4.1 and Figure 4.2 show the topology of the corporate feed and a 2-way multi-section Wilkinson power divider used for the design of the uniform and non-uniform beamforming networks respectively.

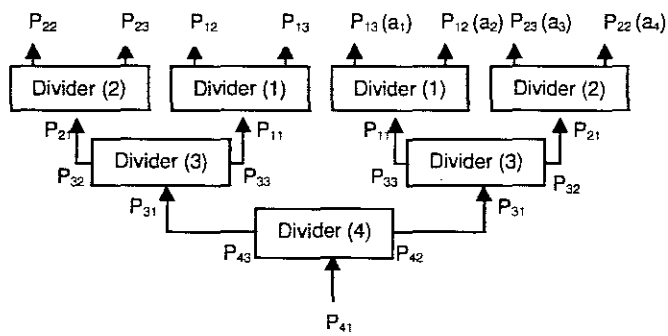

Figure 4.1: Corporate feed topology.

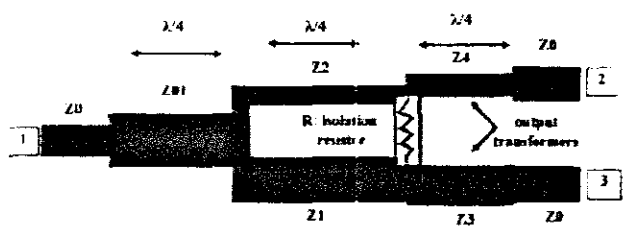

Figure 4.2: 2-way multi-section Wilkinson power divider.

A single section equal-split Wilkinson power divider was designed and simulated. The analyses showed that such a design yields a narrow-band frequency response and did not achieve the BW required for a $|S_{11}| < -25$ dB. This is due to the quarter-wave transformer arms of the divider ensuring only a matched condition at the design frequency of 10 GHz. A multi-section 3-dB Wilkinson divider was then opted for, thus yielding a broader frequency response. The parameters in Figure 4.2 are given in Table 4.3 and were calculated with the power ratio $K = 1$ using the following equations (Ahn and Wolff, 2000:1137-1140):

$$Z_{01} = Z_0\left(\frac{K}{1+K^2}\right)^{0.25} \tag{4-3}$$

$$Z_1 = Z_0\left(\frac{1+K^2}{K^5}\right)^{0.25} \tag{4-4}$$

$$Z_2 = Z_0\left(K^3\left(1+K^2\right)\right)^{0.25} \tag{4-5}$$

$$Z_3 = \frac{Z_0}{\sqrt{K}} \tag{4-6}$$

$$Z_4 = Z_0\sqrt{K} \tag{4-7}$$

$$R = Z_0\left(\frac{1+K^2}{K}\right) \tag{4-8}$$

where Z_0 is the characteristic impedance, R is the isolation resistor which was omitted to ease the layout of the feed. The power ratio between ports 2 and 3 is $K^2 = P_{n3}/P_{n2}$, where n is an integer indicating power divider 1, 2, 3, and 4.

Table 4.3: Calculated impedances for two-section equal power divider

Parameters	Impedance [Ω]	Width microstrip [mm]	Length λ
Z_0	50	0.6	N/A
Z_{01}	44.7	0.74	1/4
Z_1	69.1	0.26	1/4
Z_2	70	0.25	1/4
Z_3	54.25	0.49	1/4
Z_4	55.1	0.47	1/4

Figure 4.3 shows the impedance BW comparison between a single section, a two-section and three-section Wilkinson power divider using the T-line models in MWO for a $|S_{11}| < -25$ dB. The frequency response in Figure 4.3 shows that a two-section Wilkinson power divider meets the $|S_{11}| < -25$ dB impedance BW requirement and was thus used.

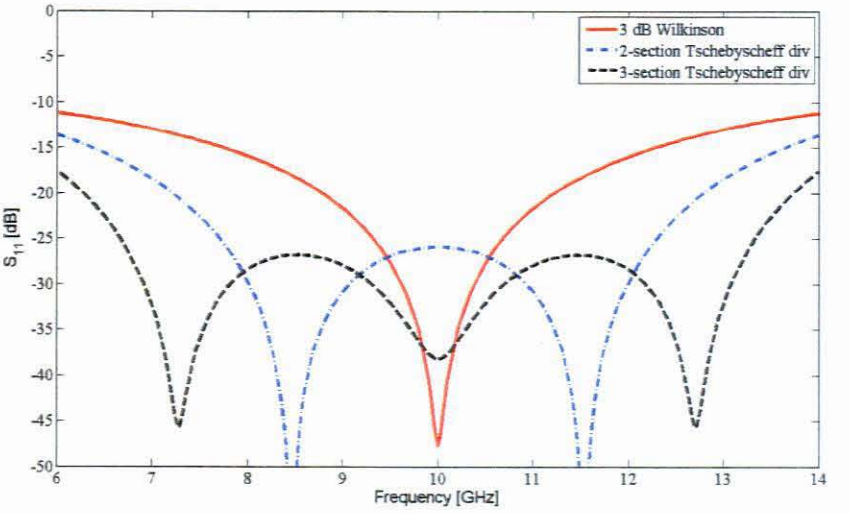

Figure 4.3: Impedance BW evaluation for power dividers.

4.2.1 Optimisation

4.2.1.1 Two-way equal power divider

It is only necessary to design one divider since the uniform beamforming network comprises identical power dividers interconnected together. A single two-section equal-split Wilkinson divider was then modelled and optimised using microstrip line models in MWO. The simplex optimisation technique, which is based on the "Nelder-Meade optimiser", was employed. The variables optimised were the widths of the microstrip lines. The optimisation was done for the performance goal set as $|S_{11}| < -40$ dB over the frequency range 8 GHz to 12 GHz. However, it is possible to achieve a Tschebyscheff frequency response for the input return loss by correctly choosing the parameters in Figure 4.2. The microstrip widths given in Table 4.3 were used as a starting point for optimisation. The optimised microstrip model with line widths and lengths for the single two-section 3-dB Wilkinson divider and S-parameters are shown in Figure 4.4(a). The input reflection loss and transmission coefficients are shown Figure 4.4(b) and Figure 4.4(c) respectively.

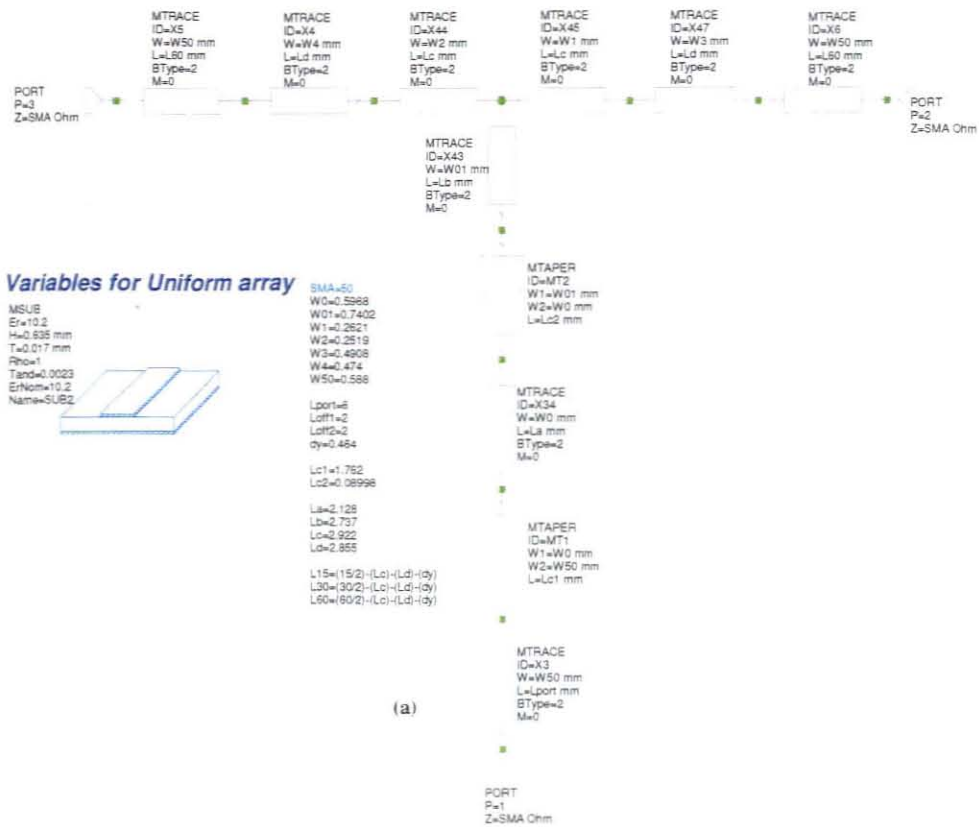

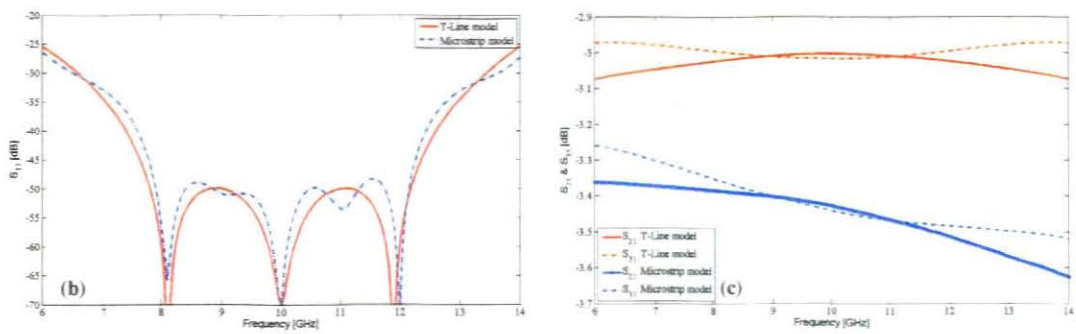

Figure 4.4: S-paramters for two-way 3-dB Wilkinson divider (a) Microstrip model, (b) $|S_{11}|$ and (c) $|S_{21}|$ and $|S_{31}|$.

4.2.1.2 Eight-way equal-power divider

When keeping the lengths from input port to all output ports identical, the beam position is independent of frequency (squintless) as well as the spacing between the array elements. This condition contributes to a broadband array design (Garg *et al.*, 2001:720). The single 2-way divider was used back-to-back to form the 8-way equal Wilkinson power divider. To maintain the critical lengths of the quarter-wave transformers in the power dividers as well as maintaining the element spacing, the radiators are fixed at the element spacing of $\lambda_0/2$ and the line lengths of the lines with the characteristic impedance were optimised using the same simplex algorithm as was used with the single divider. The simulated input reflection and transmission coefficients are shown in Figure 4.5(a) and Figure 4.5(b) respectively. Figure 4.6 shows the MWO microstrip line model for the uniform beamforming network. The microstrip layout of the uniform beamforming network is shown in Figure 4.7.

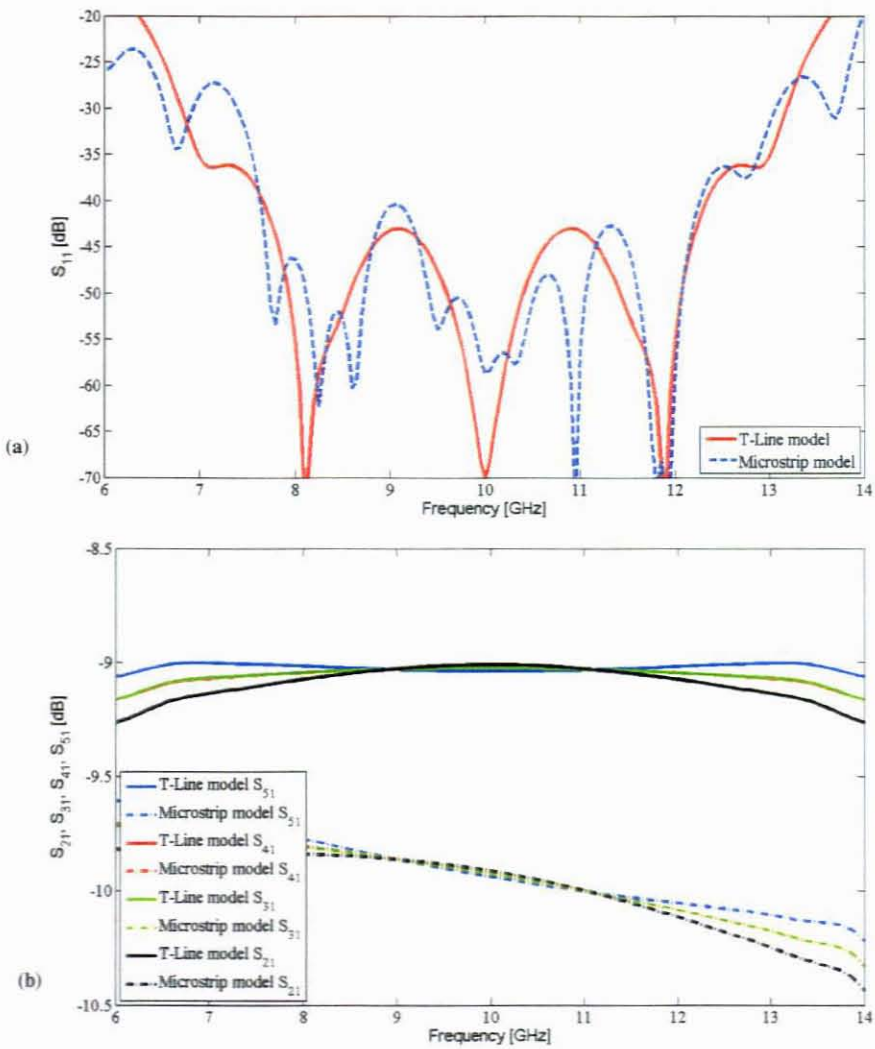

Figure 4.5: Simulated S-parameters for 8-way Wilkinson divider (a) $|S_{11}|$ and (b) $|S_{21}|$ $|S_{31}|$. $|S_{41}|$ and $|S_{51}|$.

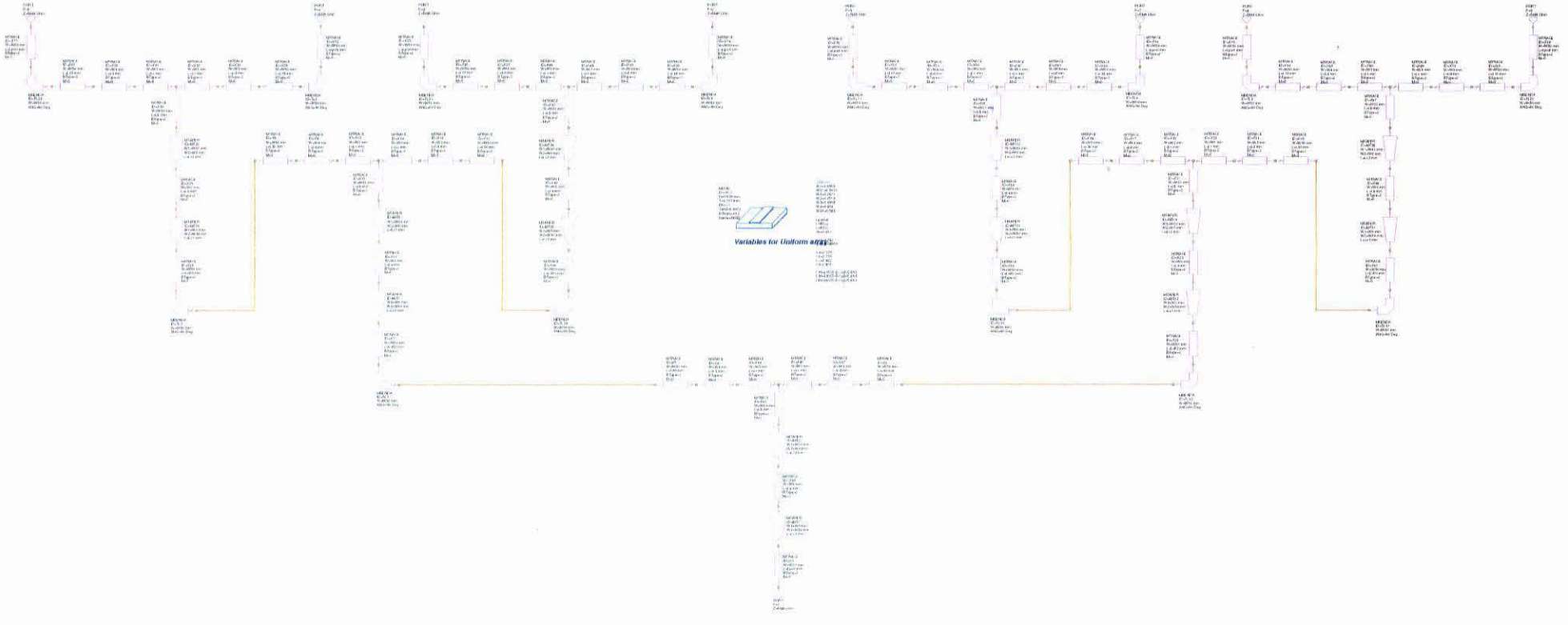

Figure 4.6: MWO microstrip model for the uniform beamforming network.

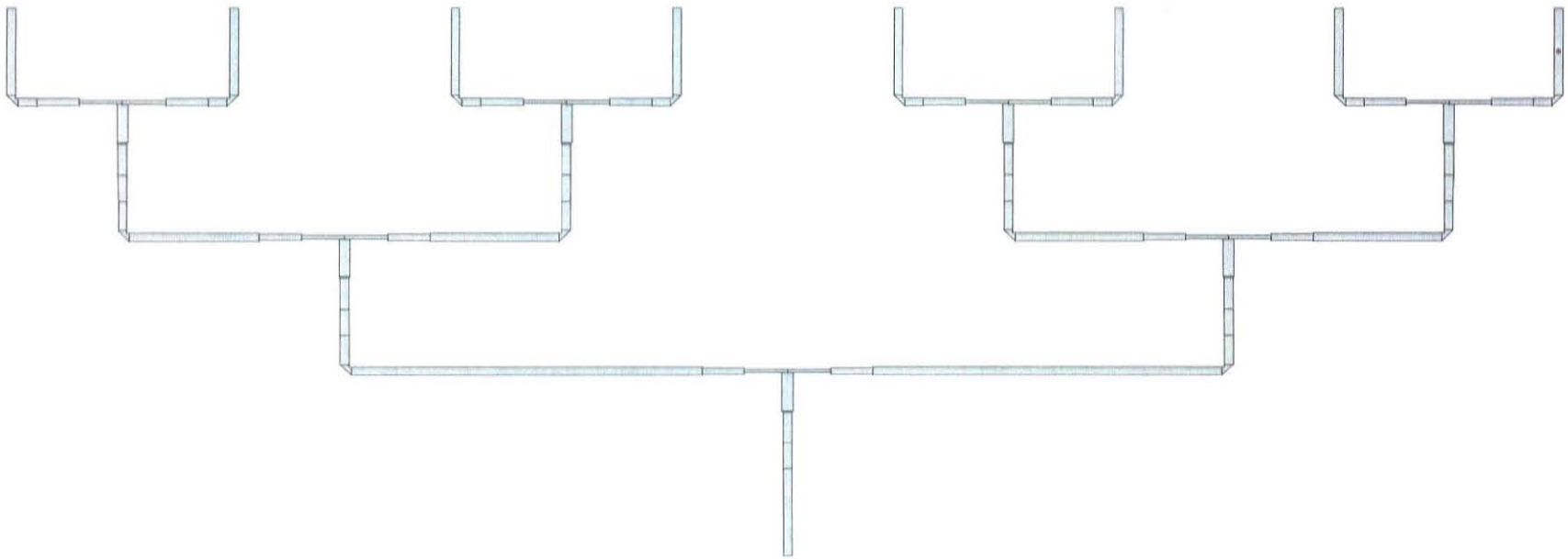

Figure 4.7: MWO microstrip layout of the uniform beamforming network.

4.2.2 Results

Since the power is not divided equally, as seen by the impedance values in Table 4.3, it is thus necessary to test the effect this amplitude excitation has on the AF over the frequency band. This test verified that the AF remains stable across the entire X-band. The final layout is seen in Figure 4.8.

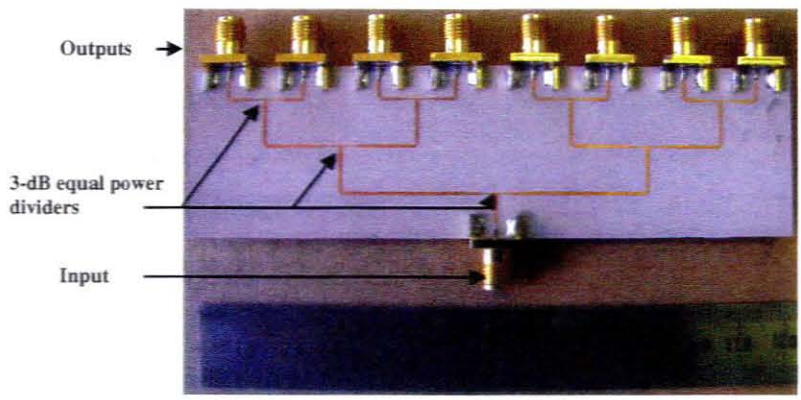

Figure 4.8: Fabricated uniform beamforming network.

The measured S_{11} for the uniform beamforming network with broadband 50 Ω loads attached to the outputs are shown in Figure 4.9. The measured results displayed a BW of 26% for a S_{11} of < -10 dB. The simulated result in Figure 4.9 takes in effect the -10 dB reflection coefficient of the coax to microstrip transition, by simulating with loads with a -10 dB reflection coefficient.

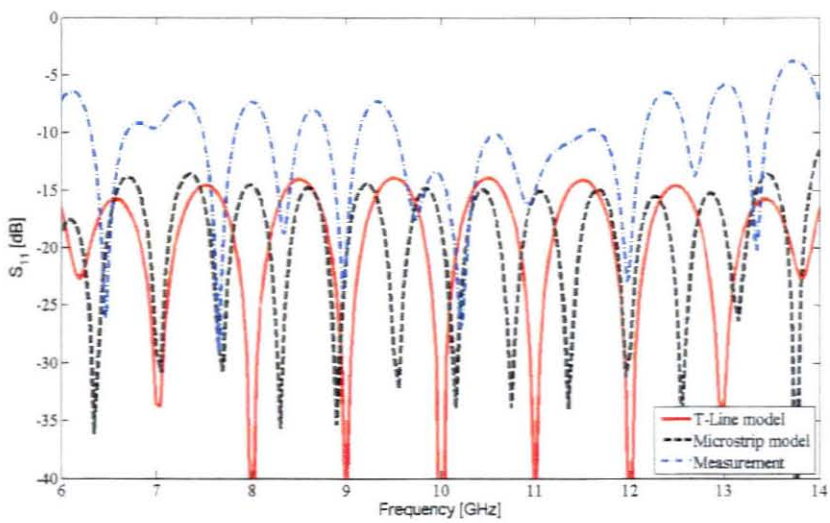

Figure 4.9: $|S_{11}|$ for uniform beamforming network

Measuring the coupling to the output ports was done by placing port 2 of the network analyser at the required output port of the beamforming network and terminating all other ports with 50 Ω broadband loads. A full 2-port measurement was performed. The coupling of only half the beamforming network is shown due to the symmetry of the network. The simulation results in Figure 4.10 displays an S_{21}, S_{31}, S_{41} and S_{51} of −10 dB across the band. The ripples in the measured transmission coefficient are due to mismatches in the beamforming network and the oscillation period being an indicator of the distance from input port to output ports.

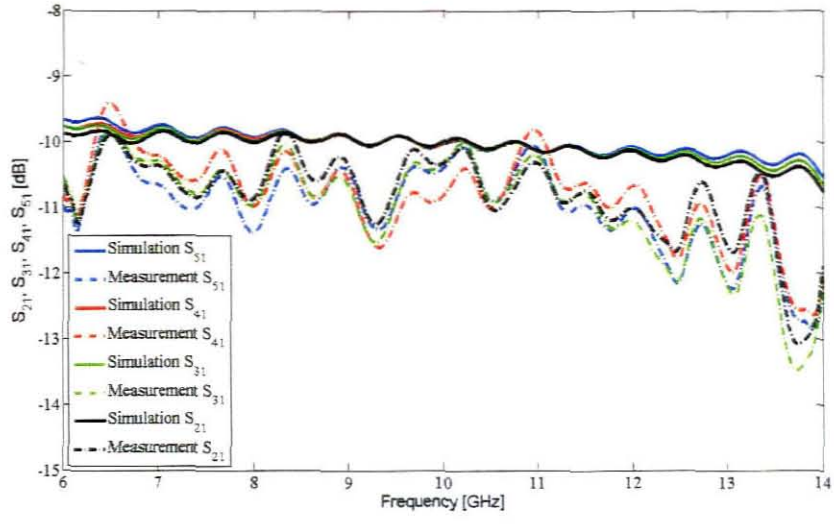

Figure 4.10: Transmission coefficients for uniform feeding network

4.3 Non-uniform beamforming network

The sidelobes of the AF for the linear uniform array are calculated to be −13 dB. However, in radar applications this is relatively high leading to false target detection through the sidelobes. It can be shown that the Tschebyscheff polynomials can be used to improve the AF, the Tschebyscheff array yields the narrowest HPBW for a specified sidelobe peak value. The synthesis of this array is based on the theory of an N-element linear array with uniform spacing with non-uniform amplitude. Two terms exist for the AF corresponding to two possible configurations for an even number of elements $2M$ and an odd number of elements $2M+1$ given by

$$(AF)_{2M}(even) = \sum_{n=1}^{M} a_n \cos[(2n-1)u] \tag{4-9}$$

$$(AF)_{2M+1}(odd) = \sum_{n=1}^{M+1} a_n \cos[2(n-1)u], \tag{4-10}$$

where M is an integer, $u = (\pi d/\lambda)\cos\theta$, d is the element spacing and a_n the excitation coefficients of the array. The parameters of the array were determined as with the uniform array. Table 4.4 and Table 4.5 give the input and output characteristics of the non-uniform array respectively.

Table 4.4: Input parameters for non-uniform beamforming network

Input specifications:	
Configuration:	Linear array
Type of array:	Non-uniform Dolph-Tschebyscheff
Radiation pattern:	Broadside (max along $\theta = 90°$)
Number of elements:	$N = 8$
Element spacing:	0.5λ
SLL	–25 dB

Table 4.5: Output characteristics for non-uniform beamforming network

Output of program	
AF directivity:	8.5555 dB or 7.1705 dimensionless
AF number of maxima between along $\theta = 0 - 180°$	1
AF theta max at	$\theta = 90°$
AF HPBW	15.4126°
Excitation coefficients	$a_1 = 6.3408$ $a_2 = 5.3416$ $a_3 = 3.7047$ $a_4 = 2.3958$
Excitation coefficients (Normalised to centre of the array)	$a_1 = 1.0000$ $a_2 = 0.8424$ $a_3 = 0.5843$ $a_4 = 0.3778$

As with the uniform beamforming network, it was only necessary to design half the beamforming network due to its symmetry. Table 4.5 shows the amplitudes for port 3 and port 2 of divider 1 and 2, given by the excitation coefficients a_1, a_2, a_3 and a_4. After determining these coefficients, the power ratios between the output ports of the dividers are calculated as $K^2 = P_3 / P_2$ to give a tapered distribution across the array. It was discovered that it would be impractical to implement the –25 dB SLL Dolph-Tschebyscheff beamforming network on microstrip with the substrate properties at hand. This was because the power ratio of divider 3 would have been too big and thus the lines too thin to implement. Therefore, the characteristic impedance of the entire network was lowered to 35 ohm and then matched to the 50 ohm feeding lines at the input and output ports using a two-section Tschebyscheff quarter-wave transformer with impedance values shown in Figure 4.11.

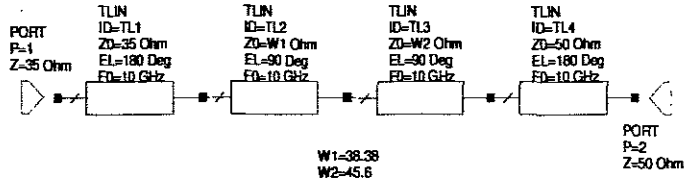

Figure 4.11: Two-section quarter-wave transformer

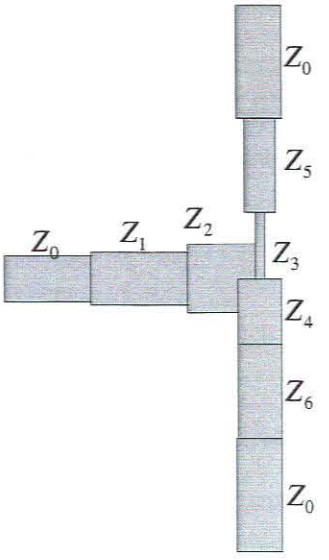

Figure 4.12: MWO microstrip layout for two-section Dolph-Tschebyscheff divider

Figure 4.12 shows one of the four two-section Dolph-Tschebyscheff models simulated in MWO. The Dolph-Tschebyscheff dividers in particular impose many physical discontinuities due to the impedance transformations within the divider. It is practically unattainable to reduce the electrical effects caused by these discontinuities by normal impedance matching. Therefore reflection losses will occur. In microstrip feeds these discontinuities cause surface waves and spurious radiation. Spurious radiation is fairly uncontrolled and adds to co-polar SLLs in certain directions and increase the total energy in the cross-polar radiation pattern, thus reducing the antenna gain. This unwanted radiation can be partially suppressed by using mode-suppression pins or microwave absorbent films placed close to the discontinuities. No effort was made to reduce these unwanted radiations. With reference to Figure 4.1, the calculated parameters for the dividers 1, 2, 3 and 4 are given in Table 4.6.

Table 4.6: Calculated impedances for non-uniform beamforming network

Divider 1			
Parameter	**Ohm Ω**	**Width (mm)**	**Length λ_g**
Z_0	35	1.16	N/A
Z_1	32.32	1.31	1/4
Z_2	26.22	1.82	1/4
Z_3	46.79	0.68	1/4
Z_4	37.3	1.03	1/4
Z_5	37.31	1.01	1/4
Z_6	35.13	1.12	1/4
Divider 2			
Parameter	**Ohm Ω**	**Width (mm)**	**Length λ_g**
Z_0	35	1.16	N/A
Z_1	33.15	1.29	1/4
Z_2	27.91	1.71	1/4
Z_3	60.44	0.24	1/4
Z_4	35.18	1.11	1/4
Z_5	38.86	0.79	1/4
Z_6	35.22	1.13	1/4
Divider 3			
Parameter	**Ohm Ω**	**Width (mm)**	**Length λ_g**
Z_0	35	1.16	N/A
Z_1	32.61	1.25	1/4
Z_2	27.03	1.58	1/4
Z_3	71.02	0.19	1/4
Z_4	31.83	1.21	1/4
Z_5	39.62	0.83	1/4
Z_6	33.96	1.16	1/4

Table 4.6: Continued.

Divider 4			
Parameter	**Ohm Ω**	**Width (mm)**	**Length λ_g**
Z_0	35	1.16	N/A
Z_1	50.67	0.57	1/4
Z_2	45.25	0.72	1/4
Z_3	62.05	0.35	1/4
Z_4	62.05	0.35	1/4
Z_5	41.16	0.87	1/4
Z_6	41.16	0.87	1/4

4.3.1 Optimisation

4.3.1.1 Two-way unequal-power dividers

The same optimisation procedure as for the uniform beamforming network was followed. The four unequal-power dividers forming the 8-way unequal-power diver were optimised individually with the goal function set to $|S_{11}| < -40$ dB over the frequency band 8 GHz to 12 GHz. The widths were again optimised as with the uniform power divider case. The input reflection coefficients for the four two-way dividers are shown in Figure 4.13.

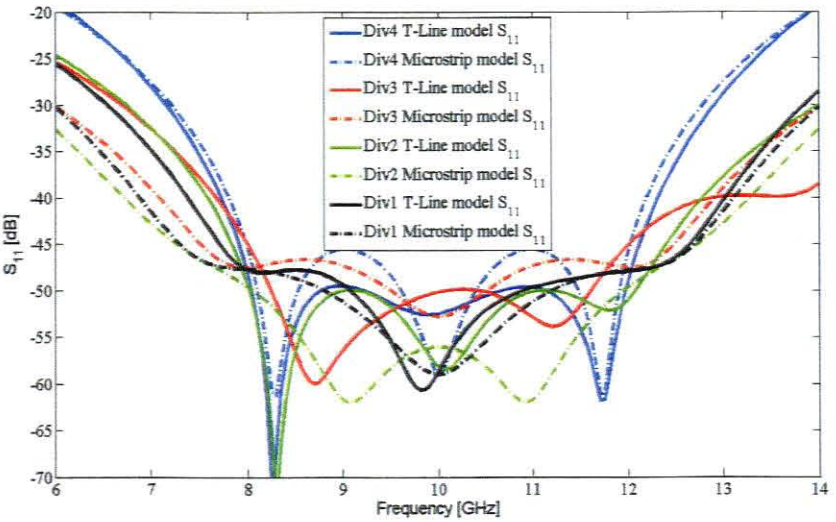

Figure 4.13: Simulated $|S_{11}|$ for 2-way unequal dividers

4.3.1.2 Eight-way unequal-power divider

The 8-way unequal power divider was formed by combining the optimised 2-way power dividers. To ensure equal phase distribution to the output ports, the 8-way unequal power divider was optimised as with the 8-way equal power divider in section 4.2.1.2. Again the radiators are fixed at the element spacing of $\lambda_0/2$ and the lines with the characteristic impedance were optimised. The simulated input reflection and transmission coefficients are shown in Figure 4.14(a) and Figure 4.14(b) respectively. Figure 4.15 shows the MWO microstrip line model for the uniform beamforming network. The microstrip layout of the uniform beamforming network is shown in Figure 4.7.

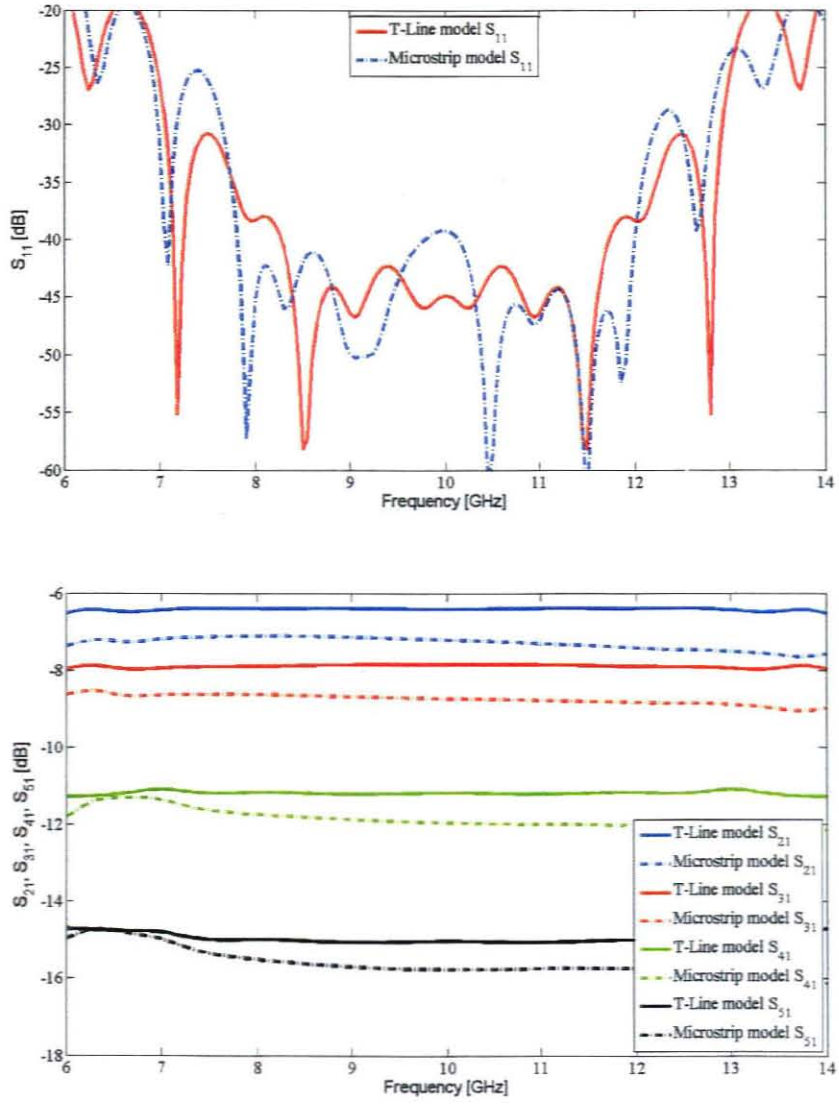

Figure 4.14: Simulated S-parameters for 8-way Wilkinson divider (a) $|S_{11}|$ and (b) $|S_{21}|$ $|S_{31}|$. $|S_{41}|$ and $|S_{51}|$.

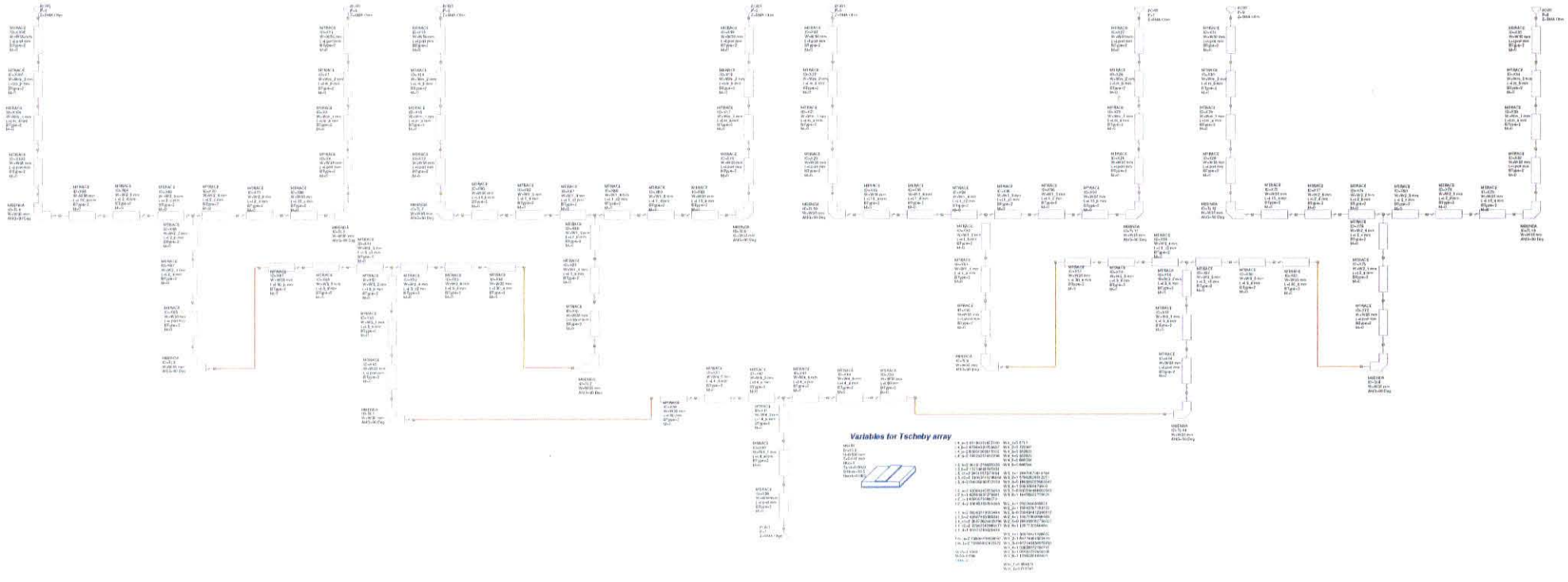

Figure 4.15: MWO microstrip model for the non-uniform beamforming network.

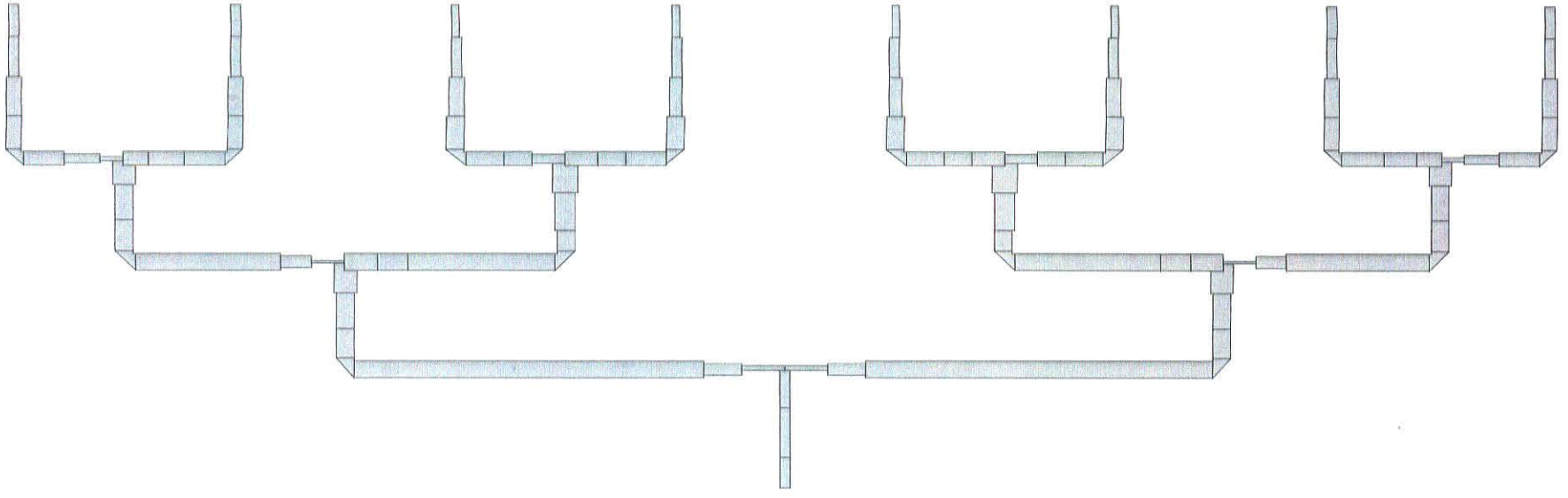

Figure 4.16: MWO microstrip layout for the non-uniform beamforming network.

4.3.2 Results

The non-uniform beamforming network is shown in Figure 4.17. SMA connectors were soldered on and the S-parameters were measured using an HP 8720ET network analyser.

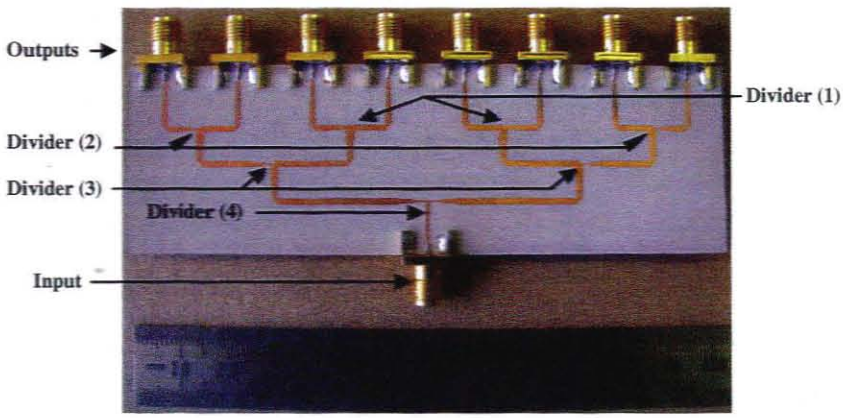

Figure 4.17: Fabricated -25 dB Dolph-Tschebyscheff beamforming network.

For both networks care was taken to ensure equal phase to all output ports. The optimisation tool in MWO was used, employing the simplex optimisation technique, which is based on the "Nelder-Meade optimiser". Figure 4.18 shows the simulated and measured S_{11} for the non-uniform beamforming network with broadband 50 ohm loads attached to all outputs. The measured result shows a poor S_{11} response with various peaks over the −10 dB reference level. The poor result is most likely to be contributed to discontinuities and errors in the feeding network, as well as the coax to microstrip transition.

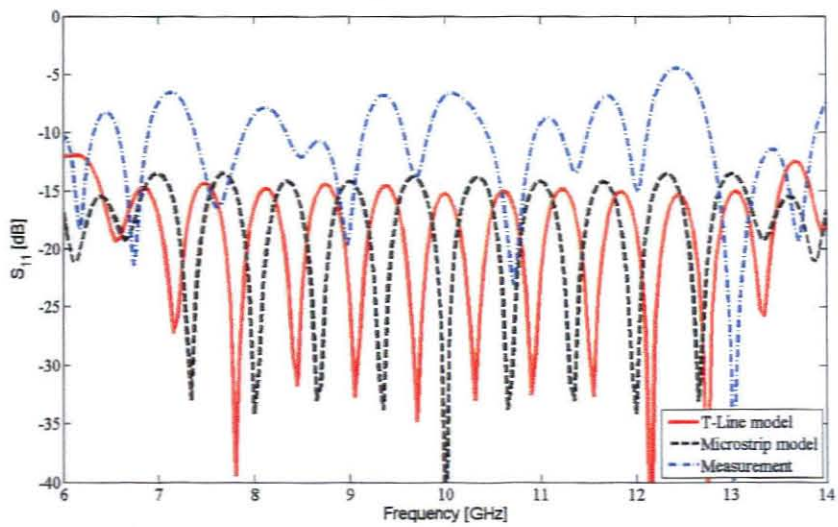

Figure 4.18: S_{11} for non-uniform beamforming network.

The simulated result in Figure 4.18 takes into effect the < −10 dB reflection mismatch of the coax to microstrip transition and includes the dielectric and conduction loss. The coupling to the output ports is presented in Figure 4.19 and shows a tapered amplitude distribution.

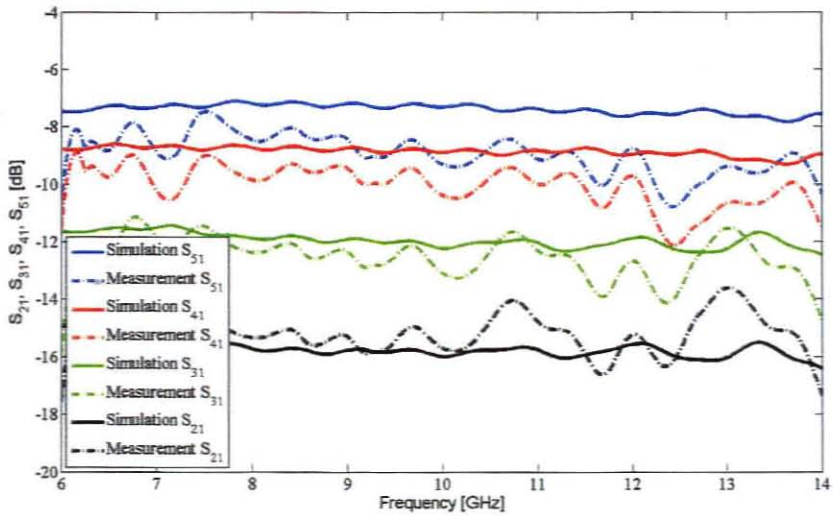

Figure 4.19: S_{n1} for non-uniform beamforming network.

The theoretical ratios K_{ij} between the power exciting ports i and j are:

$$K_{54} = \frac{a_1}{a_2} = \frac{1.0000}{0.8424} = 1.1871 \text{ or } 1.4896dB, \tag{4-11}$$

where the power ratio between ports 4 and 3 are

$$K_{43} = \frac{a_2}{a_3} = \frac{0.8424}{0.5843} = 1.4417 \text{ or } 3.1776dB. \tag{4-12}$$

The power ratio between port 3 and port 2 is given by

$$K_{32} = \frac{a_3}{a_4} = \frac{0.5843}{0.3778} = 1.5466 \text{ or } 3.7875dB. \tag{4-13}$$

The simulated power ratios shown in Figure 4.15 are K_{54sim} = 1.525 dB, K_{43sim} = 3.225 dB and K_{32sim} = 3.8 dB. Ripples in the transmission coefficient are tolerable as long as the ripples vary with respect to one another and the power ratios are maintained. This is necessary in order for the total radiation pattern to remain stable and the first sidelobes to remain below –25 dB as per design. It was observed that the measured power ratios at 10 GHz are K_{54meas} = 1.09 dB, K_{43meas} = 2.77 dB and K_{32meas} = 2.75 dB. A difference between the anticipated power ratios and the measured ratios was observed. It was anticipated that this result would affect the radiation pattern of the Dolph-Tschebyscheff array with regard to the SLL since the amplitude distribution is directly responsible for the SLL.

4.4 Delay lines

The delay line phase shifter was implemented because of its simplicity, accurate prediction of the amount of phase required and broadband characteristics. Since the array is passive, each radiating element is fed with a delay line which is progressively longer than the preceding element. To predict the location of the AF maximum, equation (4-14) can be used as

$$\psi = kd\cos\theta + \beta\big|_{\theta=\theta_0} = kd\cos\theta_0 + \beta = 0, \tag{4-14}$$

and solving for

$$\beta = -kd\cos\theta_0. \tag{4-15}$$

Taking the progressive phase as $\beta = 45°$, the separation distance as $d = \lambda/2$ and the wave number $k = 2\pi/\lambda$ and solving for θ_0, gives a direction where maximum radiation occurs as $\theta_0 = \theta_{max} = 14.5°$. Figure 4.20 shows the 45° delay line network. The overall dimensions are 15 mm by 120 mm.

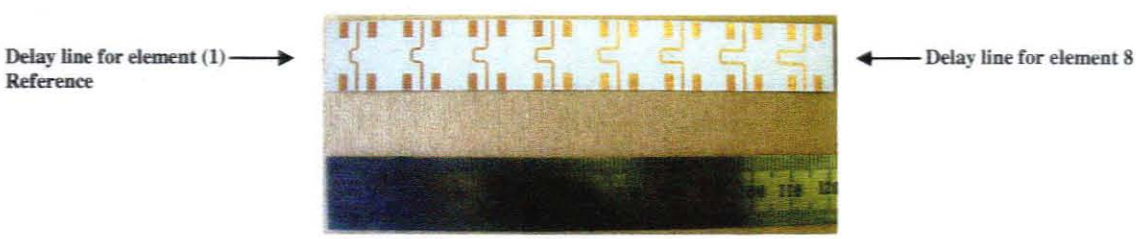

Figure 4.20: Fabricated delay line phase shifter.

4.4.1 Results

The unwrapped phase simulated in MWO is shown in Figure 4.21. The differential phase between each line is 45° at the centre frequency.

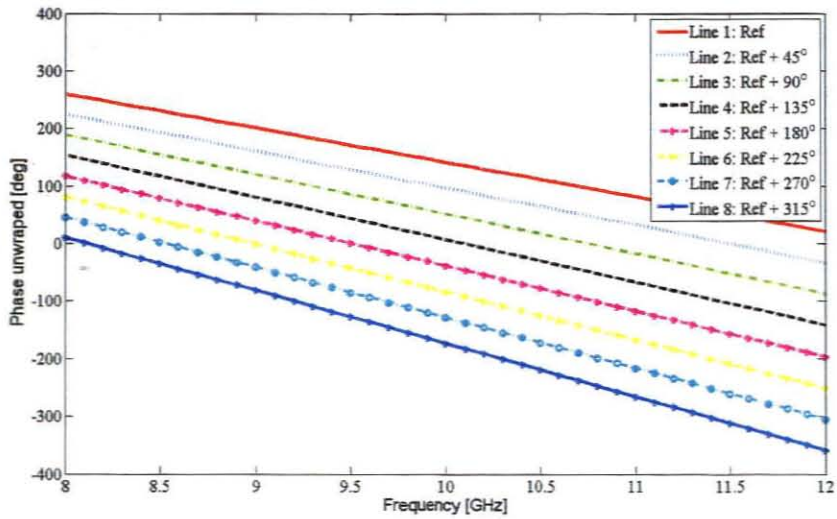

Figure 4.21: Fabricated delay line.

To investigate the effect on the far-field pattern due to a change in excitation phase, a simulation in FEKO was performed. The elements were excited with equal amplitude and the progressive phase incremented in steps of 45°. The total radiation pattern of the 8-element array is illustrated in Figure 4.22 which shows the beam scanning effect caused by a change in excitation phase.

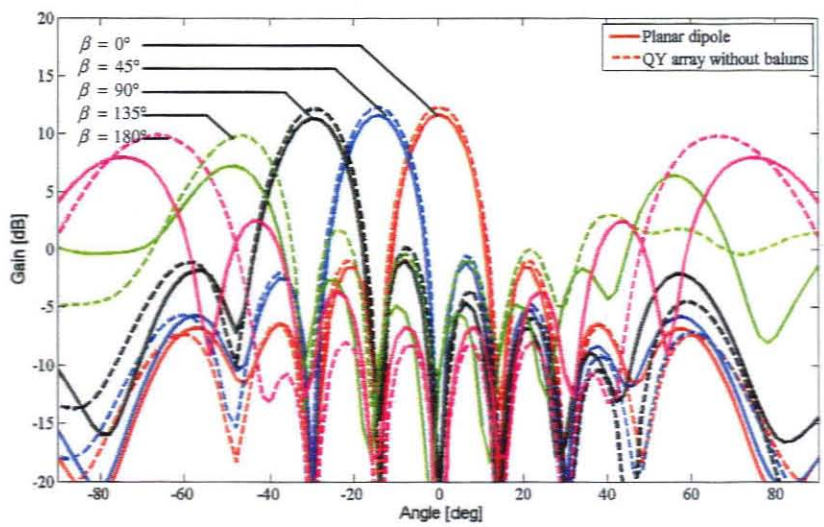

Figure 4.22: Simulated radiation pattern for $\beta = 0°, 45°, 90°, 135°$ and 180°.

Looking at Figure 4.22 it is evident that, as β increases, the beam is directed towards the end-fire direction. This is not the only visible effect, since the beamwidth also increases with an increase in β. This can be explained by a term called the "beam broadening factor", where the beamwidth and directivity are calculated by multiplying the beamwidth of a uniform array with a pre-determined beam-broadening factor. The direction where maximum radiation takes place for the progressive phase $\beta = 0°, 45°, 90°, 135°$ and $180°$ corresponds to $\phi = 0°, -14°, -30°, -48°$ and $-74°$ respectively. The radiation pattern of importance is the pattern for $\beta = 45°$ which yielded a maximum in the direction of $\phi = -14°$. It is worth mentioning that Figure 4.22 represents the total radiation pattern of the array and the predicted angle where the maximum occurs for the AF amounts to $\theta_{max} = -14.5°$. It can be seen from Figure 4.22 that for the scan angle $\beta \geq 112°$ the gain falls noticeably compared to the other scan angles. The quasi-Yagi array is not suitable as an end-fire array since the dipoles of the quasi-Yagi elements are placed in a collinear topology as seen in Figure 3.1. The radiating pattern of the dipole element constitutes a null in the end-fire direction with respect to the array axis.

4.5 Summary

In this chapter the beamforming network that feeds the eight quasi-Yagi elements was designed, simulated, optimised, implemented and measured. A uniform beamforming network and a –25 dB Dolph-Tschebyscheff non-uniform beamforming network were investigated. A 45°delay line was also inserted for these two networks to produce a squinted beam 14° from boresight.

Chapter 5 : Final measurements

5.1 Introduction

In the previous chapters, each component of the wideband microstrip phased array antenna was designed, analysed, implemented and measured. These components include the quas-Yagi antenna as a radiating element in a linear array. A uniform and non-uniform beamforming network and a 45° delay line phase shifter were also developed. In this chapter these components are integrated to form four array antennas: a uniform broadside array, a uniform fixed scan array, a non-uniform broadside array and a non-uniform fix scan array. Matlab was used to process and plot the measured data. The S-parameters were measured using an HP 8720ET network analyser. A full two-port calibration was performed over the frequency range 6 GHz to 14 GHz with 801 points. Radiation patterns were measured in the compact antenna test range (CATR) at the University of Pretoria (UP) as well as a subsequent measurements taken in the anechoic chamber at the University of Stellenbosch (US). The absolute gains for the antennas are determined using the three-antenna method. The test setup of the anechoic chamber is shown in Figure 5.1.

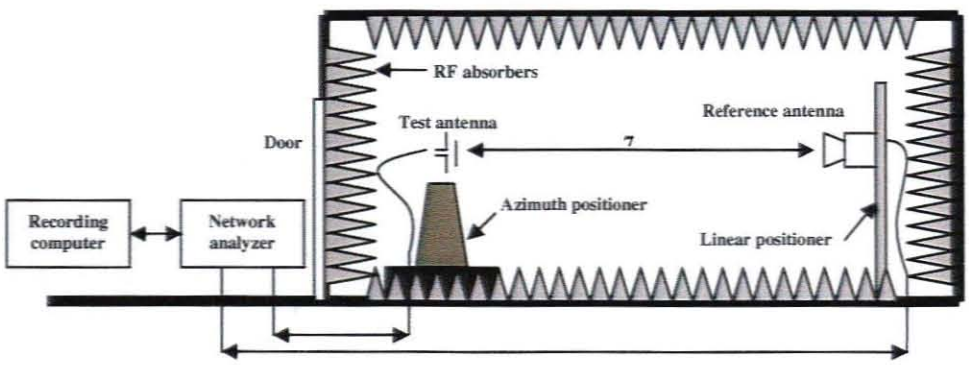

Figure 5.1: Test setup for gain and pattern measurements.

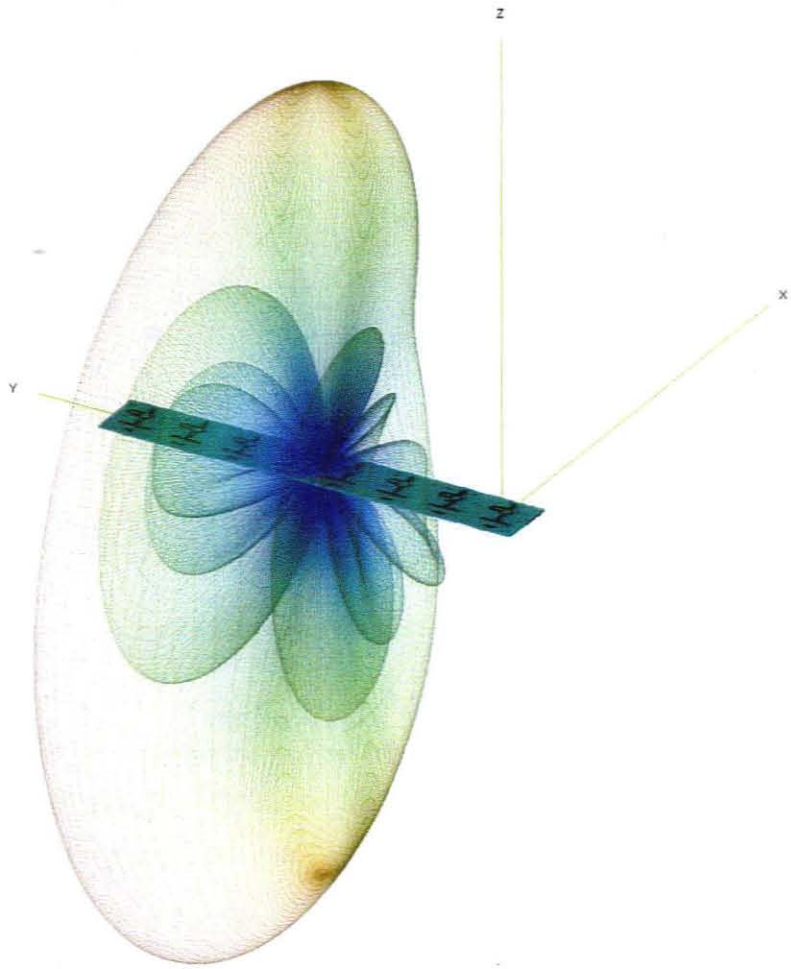

Figure 5.2: 3-D view of the quasi-Yagi array model with simulated far-field at 10 GHz.

All four array antennas generate a narrow fan beam within the E-plane as seen in Figure 5.2 above. The beamforming networks designed in chapter 4 are used to feed the array elements with predetermined amplitude and phase excitations. The result is a beam which is shaped and scanned in the E-plane. It should be mentioned that the simulated results in previous chapters do not include the fully integrated array. This was not feasible due to the complexity inherent to such a model. The elements were fed with microstrip ports with the correct amplitude and phase as would be sourced by the appropriate beamforming network.

5.2 Uniform array

5.2.1 Broadside array prototype

The uniform broadside array consists of a uniform beamforming network with eight quasi-Yagi elements spaced equally in a collinear configuration. Figure 5.3 shows the fabricated uniform broadside array. The antenna dimensions are 52 mm by 120 mm.

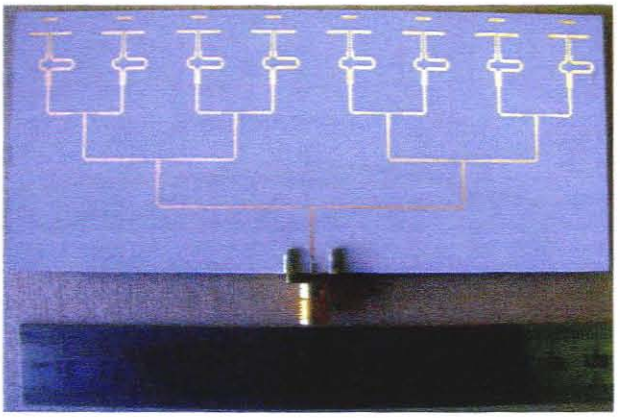

Figure 5.3: Fabricated uniform broadside array.

The S_{11} for the uniform broadside array is shown in Figure 5.4 and displays a 20% impedance BW. The poor impedance BW is due to the SMA coax to microstrip transition as well as reflections in the beamforming network.

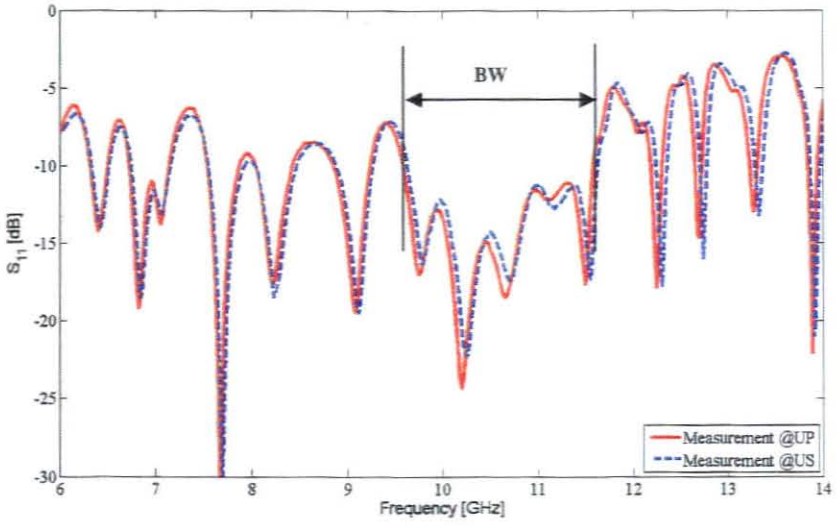

Figure 5.4: S_{11} for the uniform broadside array.

The simulated and measured gains for the uniform broadside array are shown in Figure 5.5. The simulated gain at 8 GHz, 10 GHz and 11.5 GHz are 11.5 dB, 12.8 dB and 13.4 dB respectively. The gain measured at UP revealed a gain of 10.8 dB, 12.5 dB and 10 dB at 8 GHz, 10 GHz and 11.5 GHz respectively, while the gain measured at US showed a gain of 9.7 dB, 10.9 dB and 10.7 dB at 8 GHz, 10 GHz and 11.5 GHz respectively. The discrepancies between the measurements are believed to be due to measurement errors in the chambers.

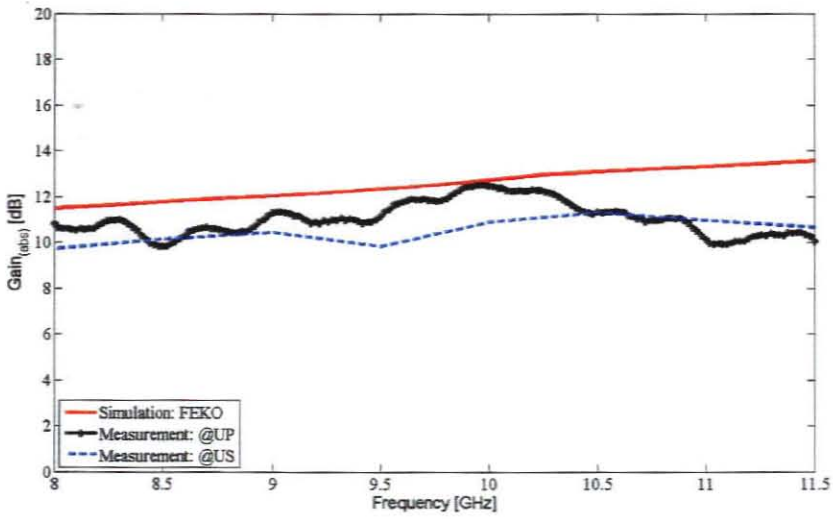

Figure 5.5: Gain for the uniform broadside array.

The radiation pattern of the uniform broadside array remains stable across the frequency band. The simulated first SLLs are at the theoretical −13 dB level with exception for the pattern at 8 GHz where the first sidelobe is approximately −12.6 dB below the main beam as seen in Figure 5.6 (a). Radiation remains broadside to the axis of the radiators as expected for this type of array. The simulated HPBW for this array at 8 GHz, 10 GHz and 11.5 GHz corresponds to 15.4°, 12.7° and 11.4° where the measured HPBW corresponds to 15.3°, 12.2° and 10.7° respectively. The simulated HPBW agrees well with the measured HPBW, however, it should be understood that the simulated results do not include the feeding network. Therefore, the losses, coupling between transmission lines, mismatches and spurious radiation associated with the beamforming network are not taken into account. These explain the differences observed in the sidelobes of the radiation patterns. An H-plane cut of the far-field pattern for the uniform broadside array is also shown in Figure 5.7. The H-plane measurements from these two test ranges follow the simulated H-plane near broadside but start to deviate from the simulation, as well as from each other, towards endfire. This can be attributed to reflections present in both the test ranges.

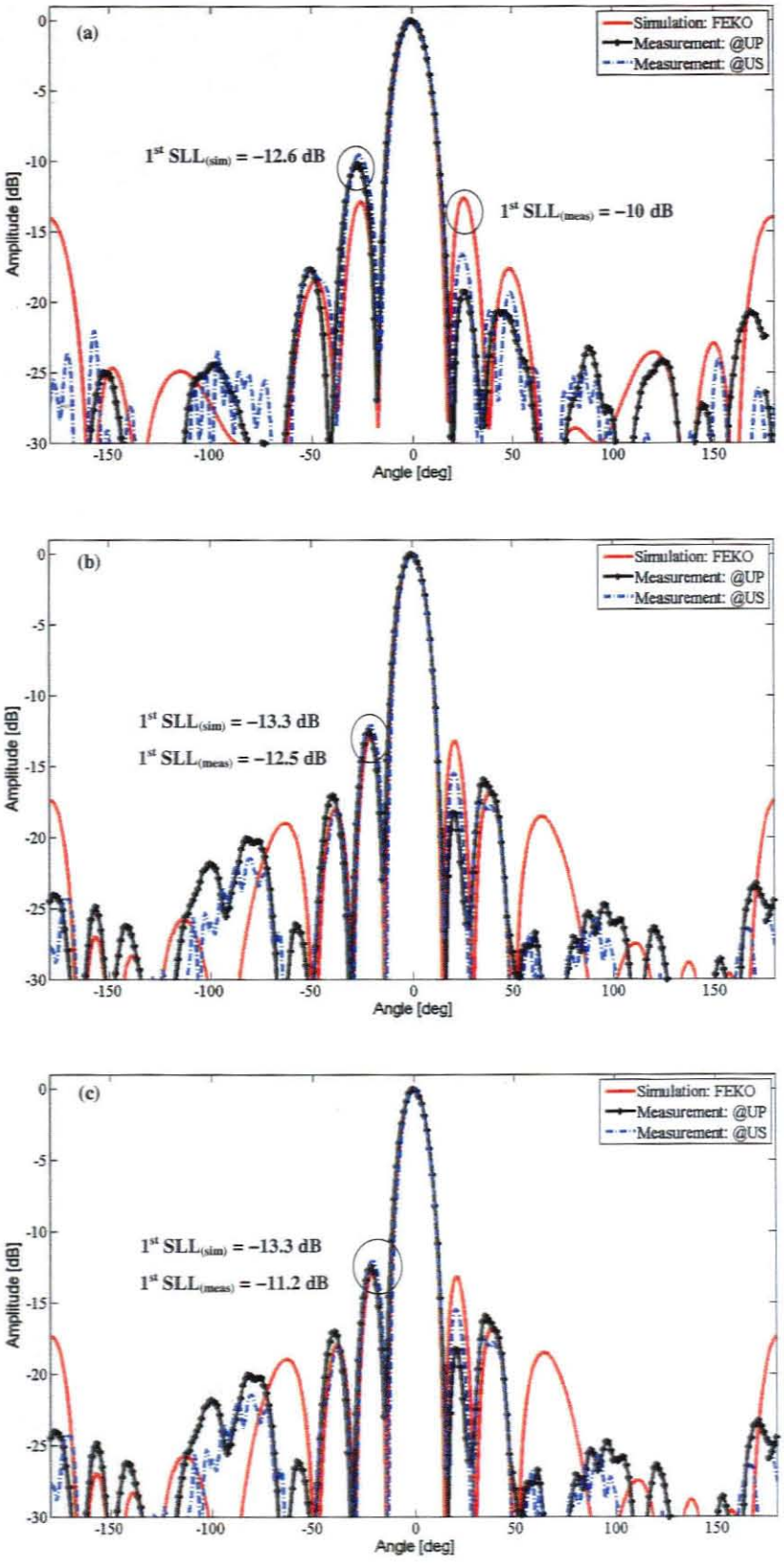

Figure 5.6: E-plane for uniform broadside array (a) 8 GHz (b) 10 GHz (c) 11.5 GHz.

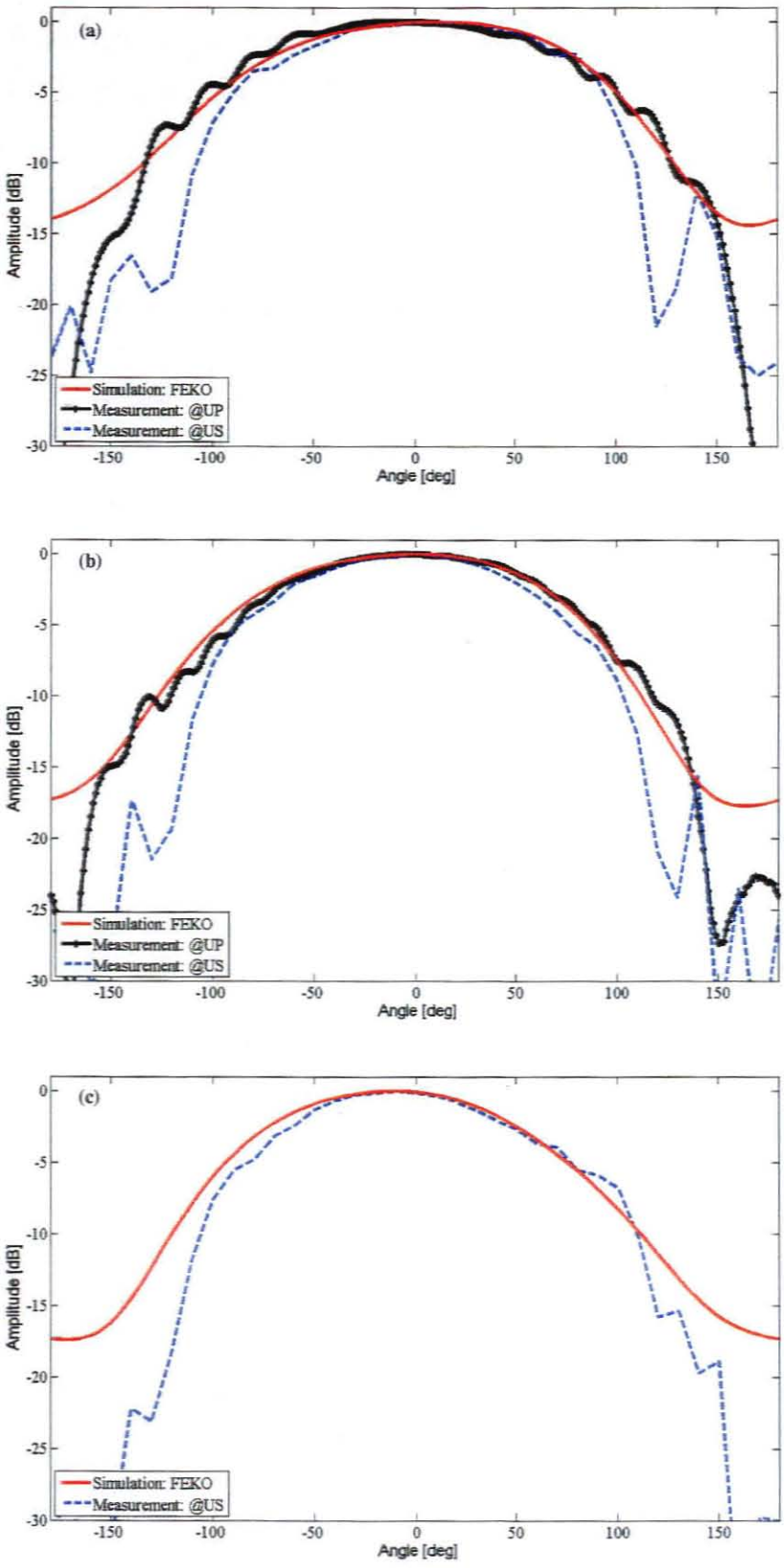

Figure 5.7: H-plane for uniform broadside array (a) 8 GHz (b) 10 GHz (c) 11.5 GHz.

5.2.2 Scanned array prototype

The uniform scanned array consists of a uniform beamforming network with the 45° delay lines feeding the eight quasi-Yagi elements spaced equally in a collinear configuration as shown in Figure 5.8. The antenna dimensions are 56 mm by 120 mm. The array was designed to generate a squinted beam 14° from boresight.

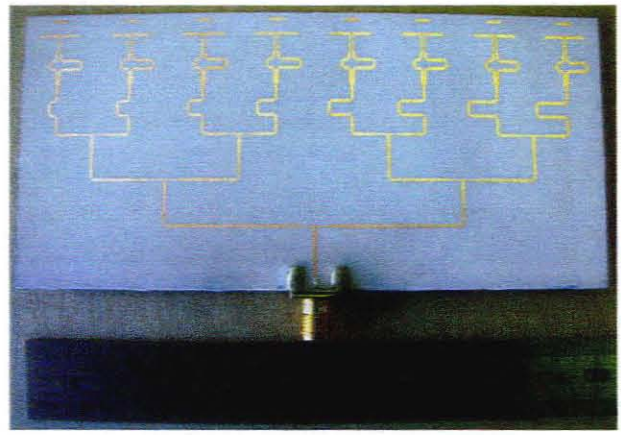

Figure 5.8: Fabricated uniform scanned array.

Figure 5.9 shows a measured BW of 10.4% from 9.76 GHz to 10.8 GHz. Several other resonances appear across the frequency band. This is due to reflections within the feeding network and discontinuities imposed by the microstrip bends and impedance changes as experienced with the uniform broadside array.

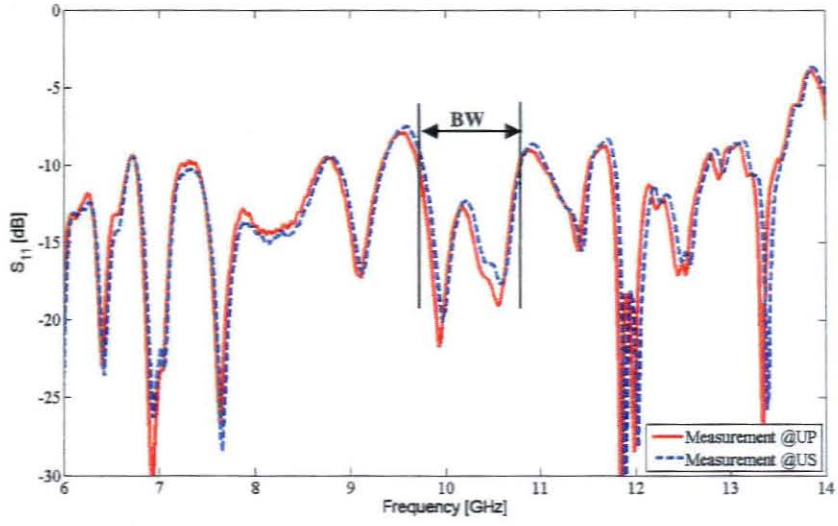

Figure 5.9: S_{11} for the uniform scanned array.

The measured gain is shown in Figure 5.10 below. The measured gain at 8 GHz, 10 GHz and 11.5 GHz as measured at the UP is 10.2 dB, 12 dB and 5.4 dB respectively.

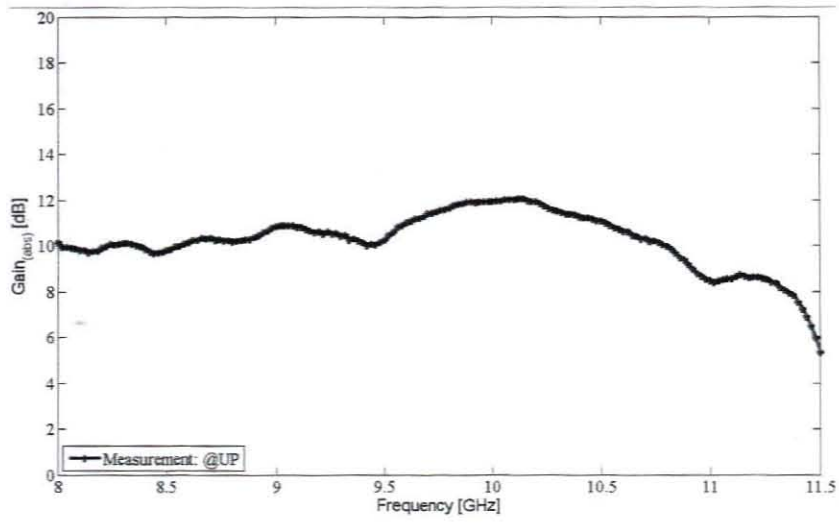

Figure 5.10: Gain for the uniform scanned array.

The calculated direction where maximum radiation occurs was at $\theta_{\max(\text{calc})} = -14.5°$. It was anticipated for maximum radiation to occur approximately at this predicted value. By looking at Figure 5.11 it is noticed that the direction where the maxima occurs was measured at $\theta_{\max(\text{meas})} = -14°$, $-14°$ and $-13°$ for the frequency points 8 GHz, 10 GHz and 11.5 GHz respectively. Figure 5.11 and Figure 5.6 also show the main beam growing narrower with an increase in frequency. This is due to the effective length of the antenna, which increases with an increase in frequency. The element spacing also increases with an increase in frequency, causing the beamwidth to decrease due to the energy being focused in the newly formed sidelobes lobes. This is also seen in Figure 6.7 of Balanis (2005:299) showing the array factor for an $N = 10$ element uniform broadside array for different element spacing. The measured HPBW at 8 GHz, 10 GHz and 11.5 GHz corresponds to 15.3°, 12.9° and 11.7°.

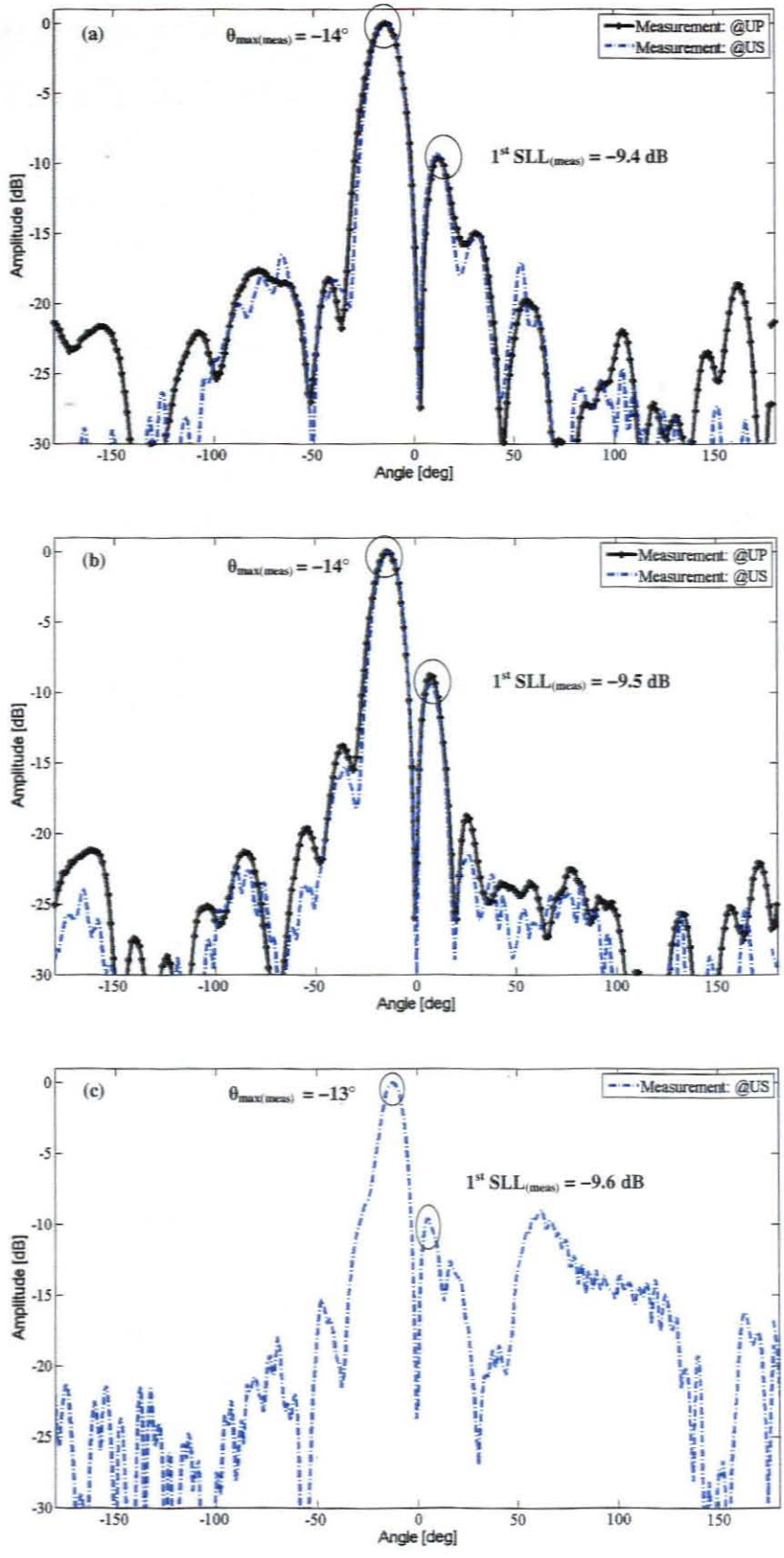

Figure 5.11: E-plane for uniform scanned array (a) 8 GHz (b) 10 GHz (c) 11.5 GHz.

5.3 Non-uniform array

5.3.1 Broadside array prototype

The non-uniform broadside array was constructed in the same manner as the uniform broadside array by combining the –25 dB Dolph-Tschebyscheff beamforming network with the eight quasi-Yagi elements. Figure 5.12 shows the fabricated non-uniform broadside array with the dimensions 52 mm by 120 mm.

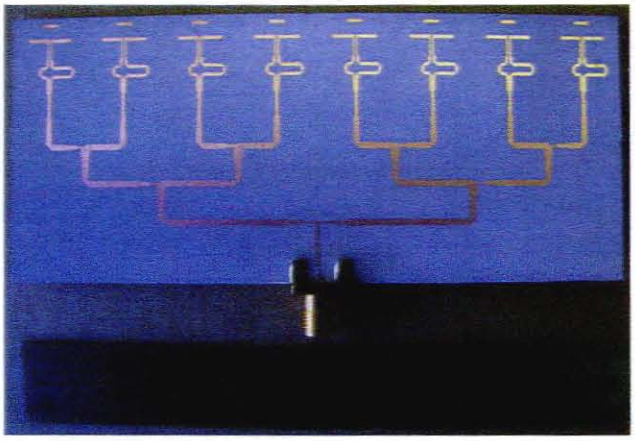

Figure 5.12: Fabricated non-uniform broadside array.

The BW performance is lower than the BW for the uniform array. Figure 5.13 shows the S_{11} from 6 GHz to 14 GHz and various resonances can be seen across the frequency band. The high input return loss is due to the discontinuities imposed by the unequal power dividers and impedance step changes within the feeding network.

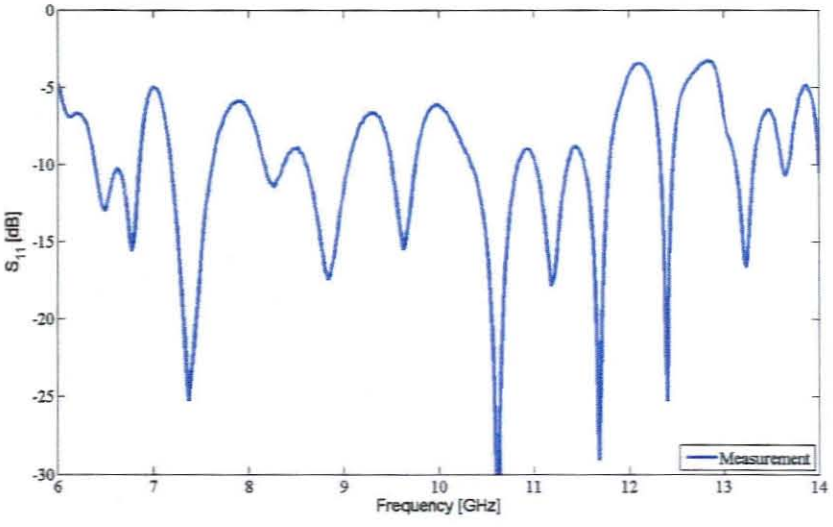

Figure 5.13: S_{11} for non-uniform broadside array.

The FEKO simulation predicted a gain of 10.9 dB 12.3 dB and 13 dB at 8 GHz, 10 GHz and 11.5 GHz respectively. The gain measured at the UP at 8 GHz, 10 GHz and 11.5 GHz are 10 dB, 11.4 dB and 9.1 dB respectively and is shown in Figure 5.14. Gain measurements taken at the US showed a gain of 8.4 dB, 9.3 dB and 9.7 dB at 8 GHz, 10 GHz and 11.5 GHz respectively. The discrepancy between the measured gains is due to measurement errors as well as the limited amount of data points taken at the US, thus limiting the resolution.

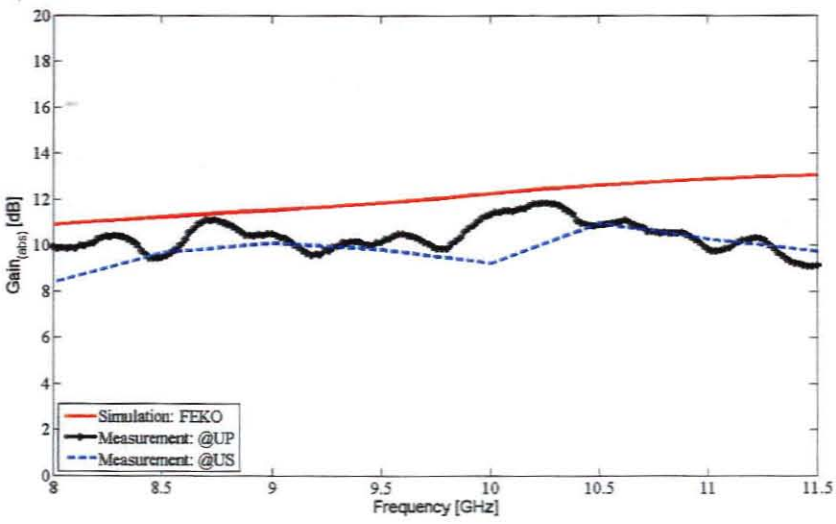

Figure 5.14: Gain for non-uniform broadside array.

The primary objective of implementing a non-uniform broadside array with a –25 dB Dolph-Tschebyscheff amplitude distribution is to lower the sidelobes to –25 dB below the main beam. This goal was achieved to some extent. Comparing the E-plane cuts of the uniform broadside array with that of the non-uniform broadside array, all SLLs of the non-uniform broadside array is considerably lower than that of the uniform broadside array. Figure 5.15 shows the E-plane cuts for the non-uniform broadside array, showing stable radiation patterns throughout the frequency band. The simulated SLLs at 8 GHz, 10 GHz and 11.5 GHz are –25.5 dB, –24 dB and –24.2 dB respectively. The measured SLLs are –20 dB, –23.5 dB and –16 dB at 8 GHz, 10 GHz and 11.5 GHz respectively. The H-plane cuts at 8 GHz, 10 GHz and 11.5 GHz are shown in Figure 5.16.

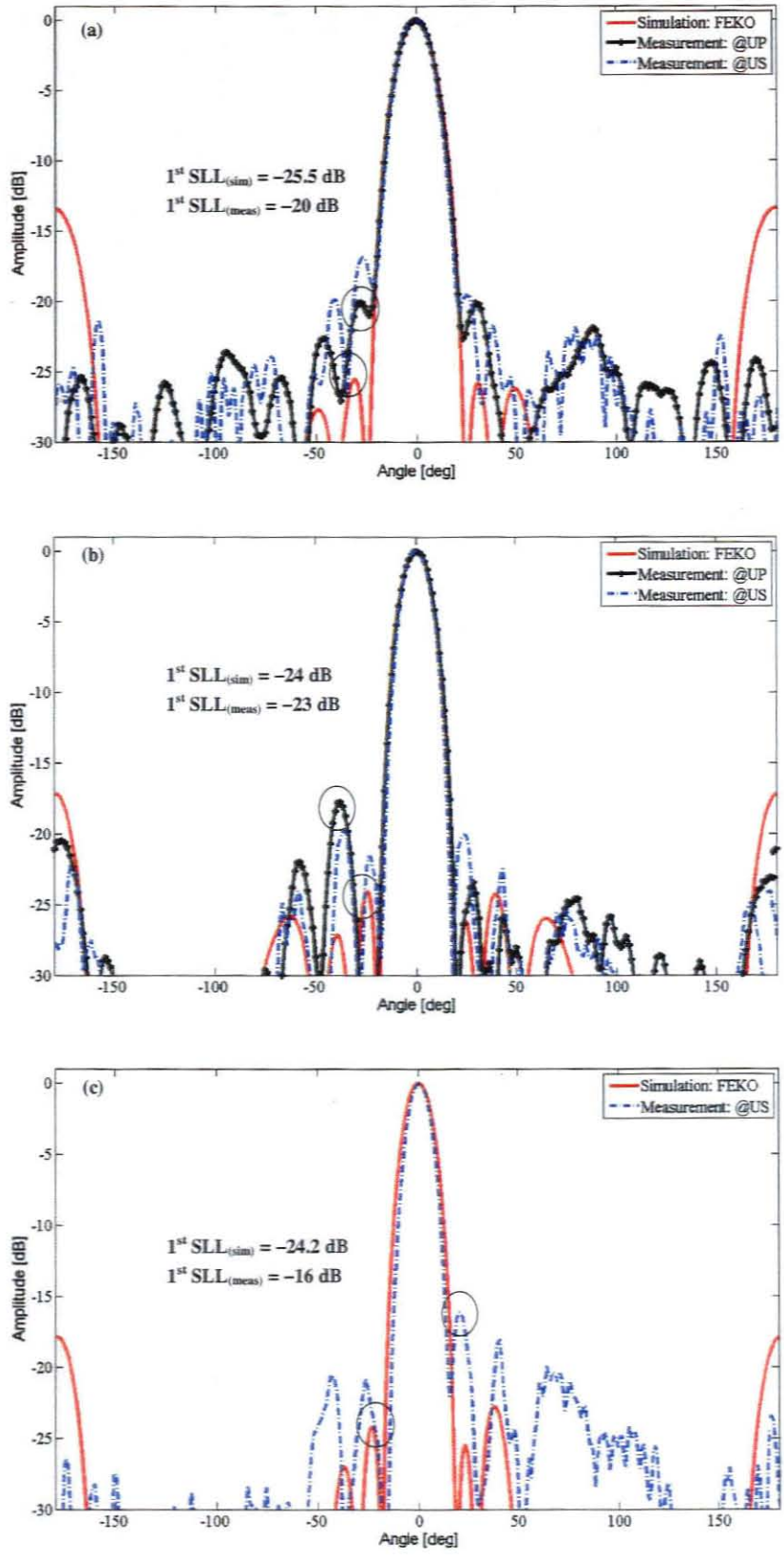

Figure 5.15: E-plane for non-uniform broadside array (a) 8 GHz (b) 10 GHz (c) 11.5 GHz.

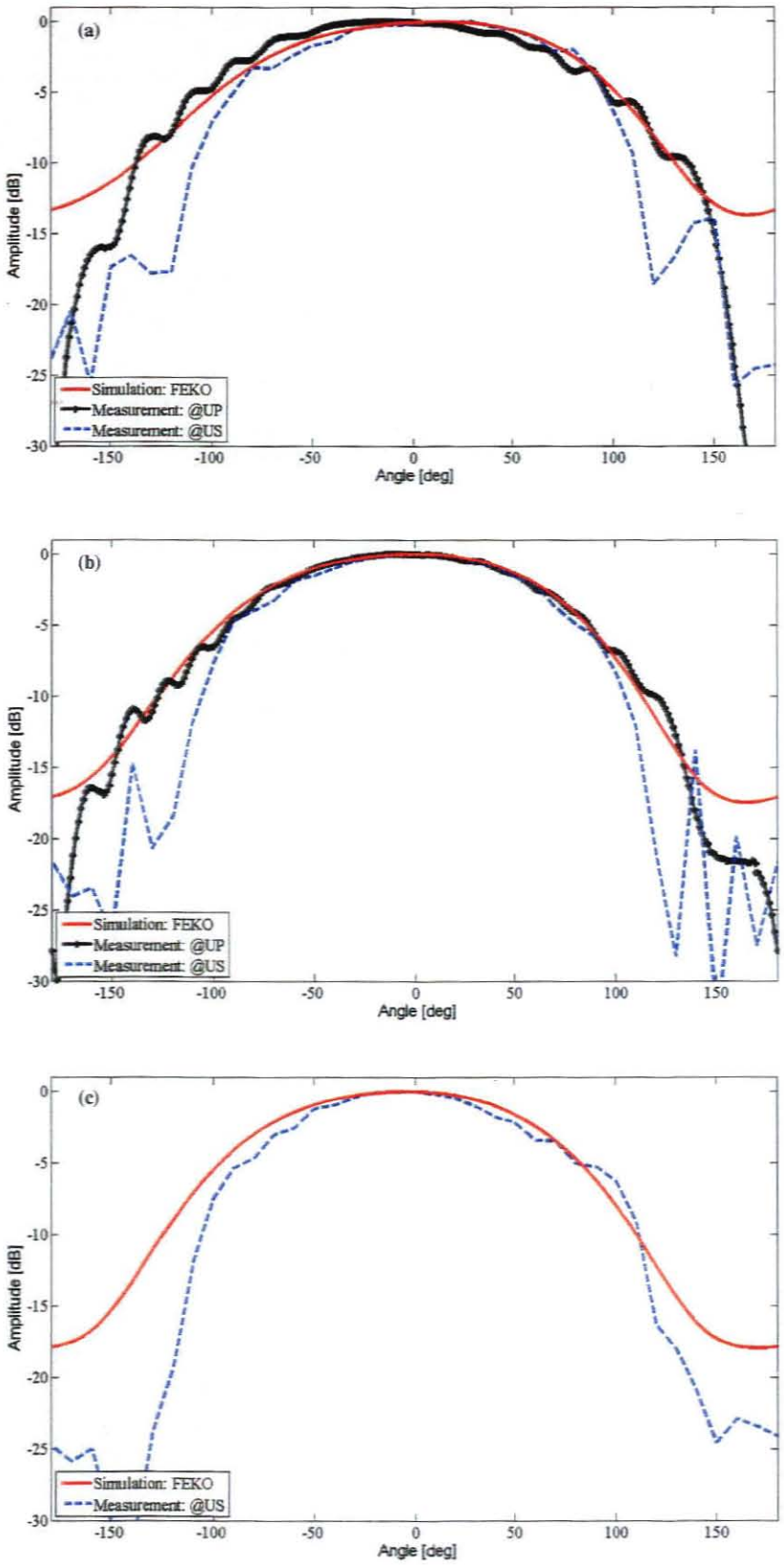

Figure 5.16: H-plane for non-uniform broadside array (a) 8 GHz (b) 10 GHz (c) 11.5 GHz.

5.3.2 Scanned array prototype

The completed non-uniform scanned array was constructed by combining the non-uniform beamforming network with eight quasi-Yagi elements spaced equally in a collinear configuration. Figure 5.17 shows the fabricated non-uniform scanned array. The antenna dimensions are 62 mm by 120 mm.

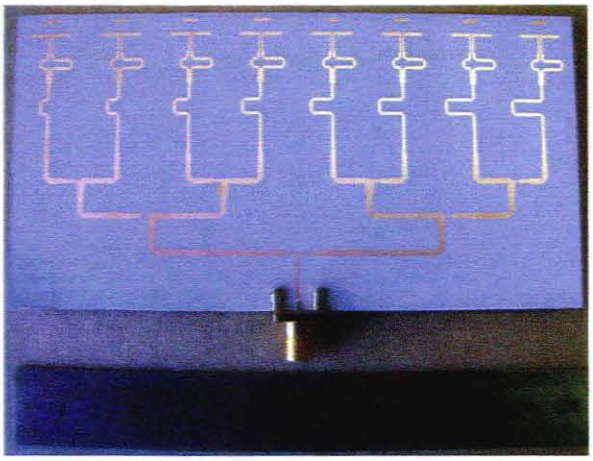

Figure 5.17: Fabricated non-uniform scanned array.

This array displayed the poorest BW performance over the frequency band. Errors in the feeding network and reflections caused by discontinuities are responsible for this result, as seen in Figure 5.18.

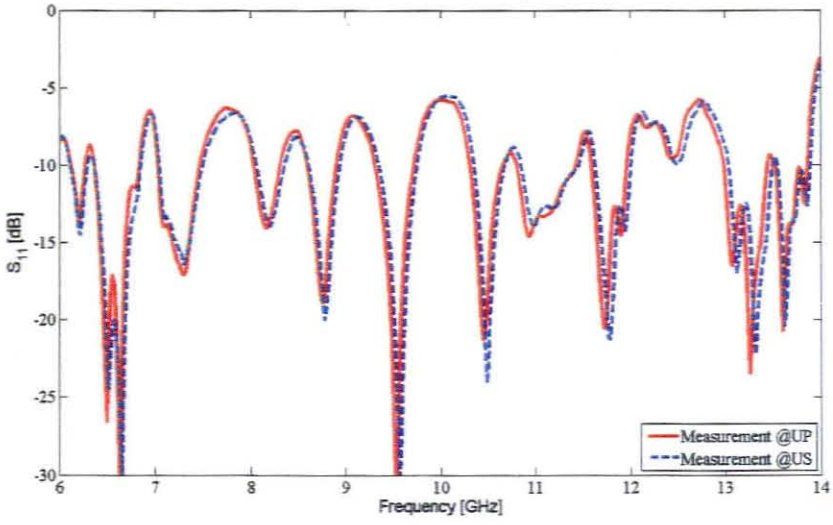

Figure 5.18: $|S_{11}|$ for non-uniform scanned array.

The measured gain is shown in Figure 5.19 below as measured at the UP. The gain at 8 GHz, 10 GHz and 11.5 GHz are 9.7 dB, 10.2 dB and 4.2 dB respectively.

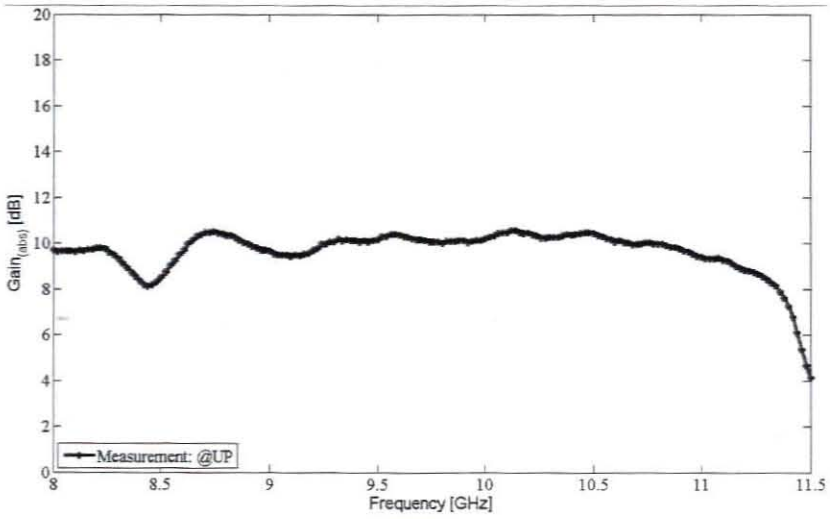

Figure 5.19: Gain for non-uniform scanned array.

Figure 5.20 shows the E-plane cuts for the non-uniform scanned array, indicating stable radiation patterns throughout the frequency band. The measured SSLs taken at UP are −20 dB, −12 dB and −10 dB at 8 GHz, 10 GHz and 11.5 GHz respectively.

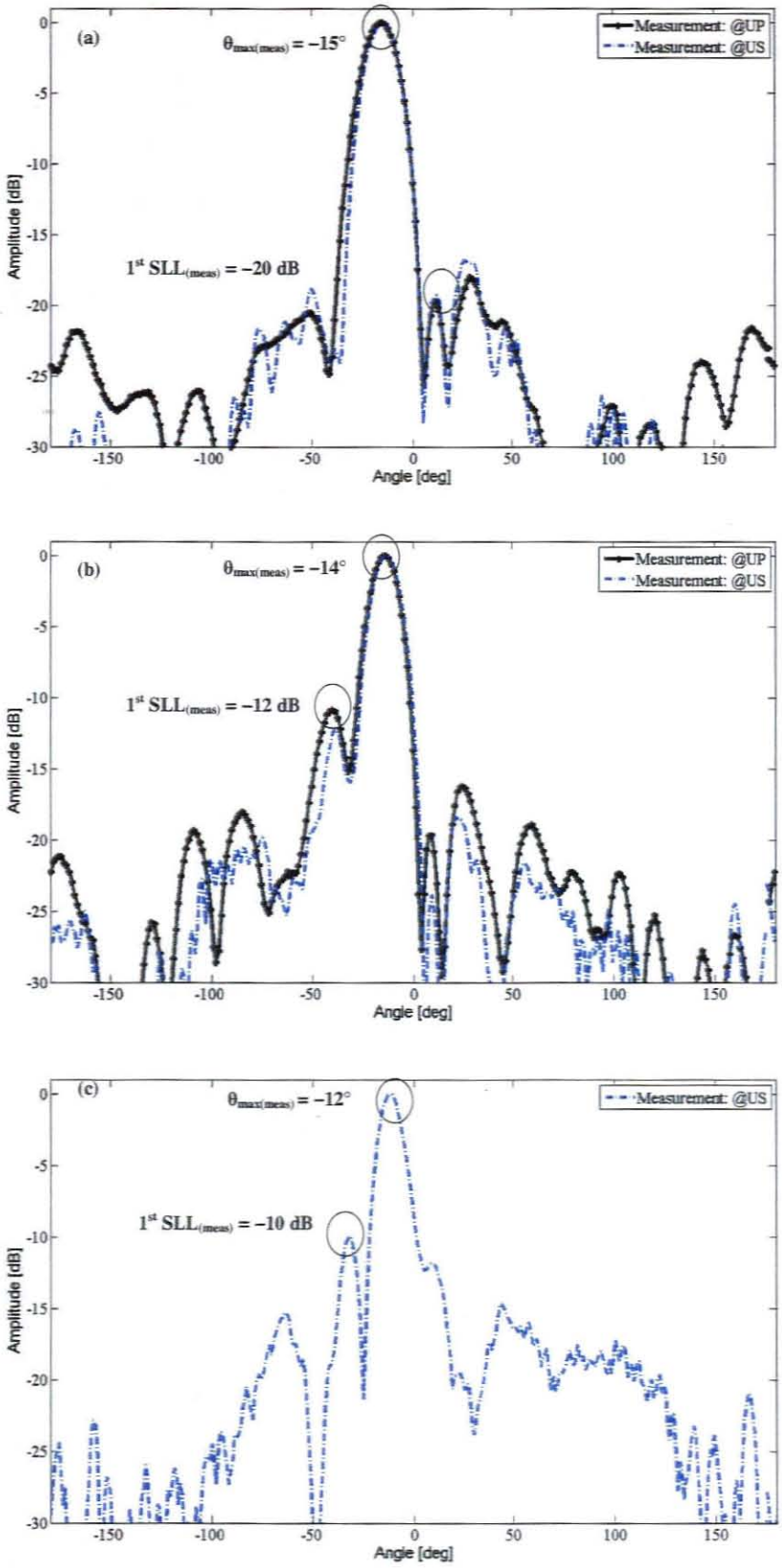

Figure 5.20: E-plane for non-uniform scanned array (a) 8 GHz (b) 10 GHz (c) 11.5 GHz.

Chapter 6 : Conclusion and recommendations

6.1 Conclusion

A wideband quasi-Yagi antenna was modelled and analysed as a suitable radiator for a wideband microstrip array antenna. The radiator showed very good simulated and measured performance across the X-band. The radiator showed an impedance BW of 50% and a gain of 3 dB to 5 dB from 8 GHz to 11.5 GHz.

A simple uniform broadside array was modelled and constructed. It showed good radiation performance across the entire frequency band form 8 GHz to 11.5 GHz. This array showed a 20% impedance BW with 11 dB of gain.

A more sophisticated non-uniform broadside array was also designed, using a –25 dB Dolph-Tschebyscheff beamforming network. This array also displayed very good radiation performance over the frequency band with approximately 11 dB of gain. The poor BW performance of the non-uniform broadside array (see Figure 5.13) is caused by discontinuities inherent to the unequal power dividers and impedance step changes. A –10 dB reflection loss caused by the SMA coax to microstrip transition is also a contributor to this poor BW performance.

Beam scanning is illustrated by delaying the excitation currents to each element by a progressive phase $\beta = 45°$, resulting in a radiating beam pointing 14° from boresight for both the uniform and non-uniform arrays. The delay lines are used as proof of concept for the implementation of a phased array antenna employing electronic phase shifters. With added time and cost this could have been implemented.

Due to the compact size and good radiation performance of the array antennas, it is highly recommended for implementation in applications requiring a light weight planar design. The small size of the array makes these antennas cost effective at X-band and higher frequency

applications. A linear array can be used to generate a narrow fan beam, as was illustrated in this research, or a 2-D array can be implemented in X-band multifunction radars.

6.2 Recommendations

Perhaps the most significant improvement to be made would be the impedance BW of the array.

Isolated Wilkinson power dividers could be used, since the isolation resistors dissipate any reflected power from the output ports of the beamforming networks.

The discontinuity imposed by the SMA coax to microstrip transition can be de-embedded from the measurements to give a true figure of the performance of the antennas.

The impedance BW of the arrays is also diminished by the reflection mismatch of the quasi-Yagi antennas as well as the mutual coupling from neighbouring elements in the array. The quasi-Yagi radiating element performance can be improved by matching and taking into consideration mutual coupling between elements.

The discrepancies between the CATR and the anechoic chamber measurements are thought to be due to reflections within the test ranges and the measurement setups. Further investigation is needed to identify the cause of these discrepancies.

Time Domain Reflectometry (TDR) measurements can be performed to investigate mismatches and discontinuities in the feeding networks.

Surface wave effects are also of concern and are worth investigating.

Bibliography

Ahn, H.R & Wolff, I. 2000. General design equations of three-port unequal power-dividers by arbitrary impedances. *Proceedings of the 2000 IEEE MTT-S Symposium digest, 11-16 June 2000.* 2:1137-1140.

Aicklen, G. H. & Tamil, L. S. 1995. Wideband planar array antenna. *Proceedings of the 1995. MILCOM Conference Record, IEEE, 5-8 Nov. 1995.* 3:1056-1060.

Alhalabi, R. A & Rebeiz, G.M. 2008. High-efficiency angled-dipole antennas for millimeter-wave phased array applications. *IEEE Transactions on Antennas and Propagation, October 2008.* 56(10):3136-3142.

Balanis, C. A. 2005. *Antenna Theory: Analysis and Design.*3rd ed. United States of America: John Wiley & Sons.

Beltran, E. C., Chavez, A. C., Torres, R. T., Garro, I. L. 2008. A wideband antenna array with novel 3dB branch-line power dividers as feeding network. *Antenna Technology: Small Antennas and Novel Metamaterials. Proceedings of the iWAT 2008 International workshop, Chiba, 4-6 March 2008.* Japan: The Institution: 267-270.

Billetter, D. R. 1989. *Multifunction Array Radar.* Norwood: Artech House.

Brookner, E. 1988. Phased array radars. In Pell, C. (ed). *Phased Array Radars.* Great Britain: Microwave Exhibitions & Publishers: 19-19.

Buch, U. V & Sharma. S. B. 2007. 8-Element Adaptive Antenna Array Synthesis with Tschebyscheff Polynomials and Algorithmic Implementation. *Telecommunications in Modern Satellite, Cable and Broadcasting Services,* Proceedings of the 2007 8th International Conference, 26-28 September 2007. The Institute: 414-418.

Chang, K., Kim, H., Hwang, K. S., Sim, H. S., Yoon, S. J. & Yoon, Y. J. 2003. A wideband dual frequency printed dipole antenna using a parasitic element. *Wireless Communication Technology, Proceedings of the 2003 IEEE Topical Conference, 15-17 Oct 2003.* The Institute: 346-347.

Cheng, S., Ojefors, E., Hallbjorner, P & Rydberg, A. 2006. Compact reflective microstrip phase shifter for travelling wave antenna applications. *IEEE Microwave and WirelessComponents Letters,* 16(7):431-433, July 2006.

Deal, W., Kaneda, N., Sor, J., Qian, Y & Itoh, T. 2000. A new Quasi-Yagi Antenna for Planar Active Antenna Arrays. *IEEE Transactions on Microwave Theory and Techniques,* 6 June 2000. 48:910-918.

Eldek, A. A. 2006. Design of double dipole antenna with enhances usable bandwidth for wideband phased array applications. *Progress In Electromagnetics Research*, 59:1-15.

Eldek, A. A., Elsherbeni, A. Z & Smith, C. E. 2005. A microstrip-fed modified printed bow-tie antenna for simultaneous operation in the C and X-bands. *Proceedings of the 2005 IEEE International Radar Conference, 9-12 May 2005,* The Institute: 939-943.

Elliott, R. 1963. The avoidance of multiple beams in Chebychev arrays. *Antennas and Propagation, IEEE Transactions on May 1963, 11(3):378-379.*

EM Wave Communications. *Ultra-wideband Antennas.* http://www.em-wise.com [02 June 2008].

FEKO. 2008(a). How to decide which numerical technique to use in FEKO. https://www.feko.info/helpcenter/how-to/how-to-decide-which-numerical-technique-to-use-in-feko [25 July 2008].

FEKO. 2008(b). How to feed microstrip lines when using finite substrates (SEP). https://www.feko.info/helpcenter/how-to/how-to-feed-microstrip-lines-when-using-finite-substrates-(sep) [31 July 2008].

Galati, G. (ed). 1993. *Advanced radar techniques and systems: The Electrical Engineering and Applied signal processing series.* United States of America: CRC Press.

García, V. C., Casaleiz, R., Segura, E. M., Otero, P., Peñalosa, C. C. 2006. Balun Effects in the Quasi-Yagi Antenna. *Proceedings of the 2006 IEEE MELECON, Benalmádena (Málaga),* 16-19 May 2006. *Spain:* The Institute: 320-323.

Garg, R., Bhartia, P., Bahl, I. & Ittipiboon, A. 2001. *Microstrip Antenna Design Handbook.* Norwood: Artech House.

Gupta, C. D. 1991. Design and Development of Wide Band Dolph-Chebyshev Antenna Array. *Antennas and Propagation Society International Symposium, 24-28 Jun 1991.* 3:1436 - 1440

Hansen, R. C. 1998. *Phased Array Antennas*. United States of America: John Wiley & Sons.

James, J. R., Hall, P. S. & Wood. C. 1981. *Microstrip Antenna Theory and Design.* United Kingdom: Peter Peregrinus.

James, J.R. & Hall, P.S. (ed). 1989. *Handbook of Microstrip antennas Volume 1.* United Kingdom: Peter Peregrinus.

James, J.R. & Hall, P.S. (ed). 1989. *Handbook of Microstrip antennas Volume 2.* United Kingdom: Peter Peregrinus.

Kan, H. K., Waterhouse, R. B., Abbosh, A. M & Bialkowski M. E. 2007.Simple Broadband Planar CPW-Fed Quasi-Yagi Antenna, *IEEE Antennas and Wireless Propagation Letters,* (6):18-20, 2007.

Kumar, G. & Ray, K. P. 2003. *Broadband Microstrip Antennas.* Norwood: Artech House.

Lai, M. I., Liu, C. F & Jeng, S. K. 2006. Design of A Multifunctional and Cost-Effective Wideband Planar Antenna Array System for Multiple Wireless Applications. *IEEE Antennas and Propagation Society International Symposium, 9-14 July 2006. The Institute*:871-874

Lee, M. J., Song, L., Yoon, S & Park, S. R. 2000. Evaluation of Directivity for Planar Antenna Arrays, *IEEE Antennas and Propagation Magazine,* June 2000. 42(3):64-67.

Li, M & Chang, K. 1999. Novel Low-Cost Beam-Steering Techniques Using Microstrip Patch Antenna Arrays Fed by Dielectric Image Lines. *Antennas and Propagation, IEEE Transactions, March 1999.* 47(3):453-457.

Lo, Y. T. & Lee, S. W. 1993. *Antenna Handbook :vol 3:* United States of America: Van Nostrand Reinhold.

Lynes, G. D. Johnson, G. E. Huckleberry, B. E & Forrest, N. H. 1974. Design of a Broad-Band 4-Bit Loaded Switched-Line Phase Shifter. *IEEE Transactions on Microwave Theory and Techniques.* June 1974. 22(6):693-697.

Mailloux, R. J. 1980. Progress in Phased Array Technology, *Microwaves, Radar and Wireless Communications.* Proceedings of the 13th International Conference, 22-24 May 2000. 1:166-169.

Mailloux, R.J. 2005. *Phased Array Antenna Handbook.* 2nd ed. Norwood: Artech House.

Miyaguchi, K., Hieda, M., Nakahara, K., Kurusu, H., Nii, M., Kasahara, M., Takagi, T & Urasaki, S. 2001. An ultra-broad-band reflection-type phase-shifter MMIC with series and parallel LC circuits. *IEEE Transactions on Microwave Theory and Techniques,* 12 December 2001. 49(12): 2446-2452.

Pell, C. (ed). 1988. *Phased Array Radars.* Great Britain: Microwave Exhibitions & Publishers.

Pozar, D. M. 2005. *Microwave Engineering.* 3rd ed. United States of America: John Wiley & Sons.

Rhea, R. 2008. Historical Highlights of Microwaves. *Microwave Journal,* 51(7):26-32, July

Rigoland, P., Drissi, M., Terret, C. & Gadenne, P. 1996. Wide-band planar arrays for radar applications. *Phased Array Systems and Technology. Proceedings of the 1996 IEEE International Symposium, Boston, MA, 15-18 Oct 1996.The Institute: 163-*167.

Rizk, J. B & Rebeiz, G.A. W-band microstrip RF-MEMS switches and phase shifters. *Microwave Symposium Digest, 2003 IEEE MTT-S International.* 3:1485-1488. 8-13 June 2003.

Rudge, A. W., Milne, K., Olver, A. D & Knight, P. (eds). 1983. *The Handbook of antenna design Volume 1.* London, UK: Peter Peregrinus.

Rudge, A. W., Milne, K., Olver, A. D & Knight, P. (eds). 1983. *The Handbook of antenna design Volume 2.* London, UK: Peter Peregrinus.

Salem, P., Wu C & Yagoub, M. C. E. 2006. Non-Uniform Tapered Ultra Wideband Directional Coupler Design and Modern Ultra Wideband Balun Integration. *Proceedings of Asia-Pacific Microwave Conference 2006, 12-15 Dec 2006. The Institute*: 803-806.

Skolnik, M. I. 1962. *Introduction to Radar Systems.* International student ed. Tokyo: McGraw-Hill.

Skolnik, M. I. 1970. *Radar Handbook.* United States of America: McGraw-Hill.

Song, H. J., Bialkowski, M. E. & Kabacik, P. 2000. Parameter study of a broadband uniplanar quasi-yagi antenna, *Microwaves, Radar and Wireless Communications. Proceedings of the 13th International Conference, 22-24 May 2000.* 1:166-169.

Tsai, F. E & Bialkowski, M. E. 2004. *An X-band tray-type spatial power combiner using uniplanar Quasi-Yaqi antennas.* 4140 0-7803-8302-8/04/$20.00 02004 IEEE

Volakis, J. L. (ed). 2007. *Antenna Engineering Handbook.* 4th ed. United States of America: McGraw-Hill.

Weinmann, F. 2005. Planar 9-Element Quasi-Yagi Antenna Array for X-Band Application. *Wireless Technology, Proceedings of the European Conference on 3-4 Oct 2005.*The Institute: 539-542.

Woo, D. S., Kim, Y G, Kim, K W. & Cho, Y. K. 2008. Design of Quasi-Yagi antennas using an ultra-wideband balun. *Microwave and optical technology letters*, 50:2068-2071, August 2008.

Wu, X. H., Kishk, A. A & Chen, Z. N. 2005. A Linear Antenna Array for UWB Applications. *Antennas and Propagation Society International Symposium, 2005 IEEE,* 3-8 July 2005. 1A: 594-597.

Yun, T. Y., Wang, C., Zepeda, P., Rodenbeck, C. T., Coutant, M. R., Li, M. & Chang, K. 2002. A 10 to 21GHz, low-cost, multifrequency, and full-duplex phased-array antenna system. *IEEE Transactions on Antennas and Propagation,* 50(5):641-650, May 2002.

Zatman, M. 1998. Low Sidelobe Taper Choice for Wideband Adaptive Arrays. *Antennas and Propagation Society International Symposium, 1998. IEEE,* 21-26 June 1998. 1:192-194.

Appendix A: Array theory

A.1 Array antennas

The total field of an array antenna is determined by the vector addition of the individual fields of the elements, assuming equal current distribution and neglecting mutual coupling. In practise mutual coupling cannot be neglected since it has an adverse effect on the array performance. To achieve very directive patterns, the individual fields need to interfere constructively in the desired directions and destructively in the unwanted directions. The attractiveness of array antennas involves the fact that the total radiation beam can be shaped and directed by altering the five control parameters which are:

- geometrical configuration of the elements
- relative displacement between elements
- amplitude excitation of the individual elements
- phase excitation of the individual elements
- the relative pattern of the individual elements.

A.1.1 Two-element array

Assume two infinitesimal horizontal dipoles as seen in Figure A.1 configured along the z-axis. Assuming no coupling between elements, the total field is given as

$$E_t = E_1 + E_2 = \hat{a}_\theta jn\frac{kI_0 l}{4\pi}\left\{\frac{e^{-j[kr_1-(\beta/2)]}}{r_1}\cos\theta_1 + \frac{e^{-j[kr_2-(\beta/2)]}}{r_2}\cos\theta_2\right\} \qquad \textbf{(A-1)}$$

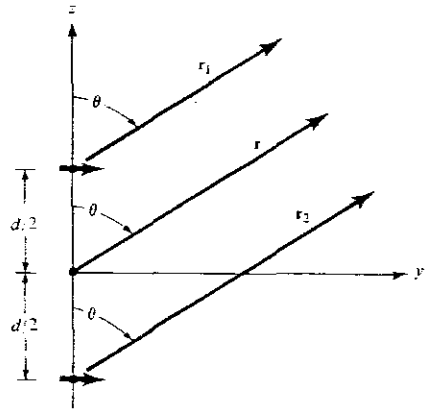

Figure A.1: Geometry of a two-element array along the z-axis with far-field observation (Adapted from Balanis, 2005:285).

with β the difference in phase excitation between the elements. The magnitude excitations of the elements remain equal. Looking at Figure A.1, assuming far-field observation, angles and distances can be written as

$$\theta_1 \approx \theta_2 \approx \theta \tag{A-2}$$

$$r_1 \approx r - \frac{d}{2}\cos\theta \tag{A-3}$$

$$r_2 \approx r - \frac{d}{2}\cos\theta \tag{A-4}$$

$$r_1 \approx r_2 \approx r \tag{A-5}$$

Through manipulation, equation (A-1) is written as

$$E_t = \hat{a}_\theta jn\frac{kI_0 le^{-jkr}}{4\pi r}\cos\theta\left\{2\cos\left[\frac{1}{2}(kd\cos\theta+\beta)\right]\right\}. \tag{A-6}$$

From equation (A-6) it is noticed that the total field of the array is equal to the field of a single element multiplied by the factor, termed the array factor (AF), and for a two-element array with constant amplitude this is given by

$$AF = 2\cos\left[\frac{1}{2}(kd\cos\theta+\beta)\right] \tag{A-7}$$

and in normalised form is given as

$$(AF)_n = \cos\left[\frac{1}{2}(kd\cos\theta + \beta)\right]. \quad \textbf{(A-8)}$$

The separation distance d and excitation phase β between the elements control the characteristics of the AF as well as the total field of the array. Thus, the total far-field of the array can be determined through pattern multiplication rule valid for identical elements. It is given as the product of the far-field of a single element, at a pre-determined reference point multiplied with the array factor of the array written as

$$\mathrm{E}_{(\mathrm{Total})} = \mathrm{E}_{(\text{single element @ ref point})} \times \mathrm{AF}. \quad \textbf{(A-9)}$$

The analysis method of achieving the AF for two identical elements can be generalised to include N-elements.

A.1.2 N-element linear array with uniform amplitude and spacing

The categories of linear arrays involve the placement of N-elements along any axis and can be excited uniformly or non-uniformly. A uniform array is an array where the elements are all identical, fed with identical amplitude and progressive phase. Looking at Figure A-2 and assuming equal amplitude and the phase of each succeeding element with a β progressive phase lead current relative to the preceding element. The AF for a uniform array with N-elements is given by

$$AF = \sum_{n=1}^{N} e^{j(n-1)\psi} \quad \textbf{(A-10)}$$

where $$\psi = kd\cos\theta + \beta. \quad \textbf{(A-11)}$$

The AF can be given in an alternative form for convenience by doing some manipulation of equation (A-10) starting by multiplying both sides by $e^{j\psi}$ as

$$(AF)e^{j\psi} = e^{j\psi} + e^{j2\psi} + e^{j3\psi} + \ldots + e^{j(N-1)\psi} + e^{jN\psi}. \quad \textbf{(A-12)}$$

Subtracting equation (A-10) from equation (2-12) results in

$$AF(e^{j\psi} - 1) = (-1 + e^{jN\psi}). \quad \textbf{(A-13)}$$

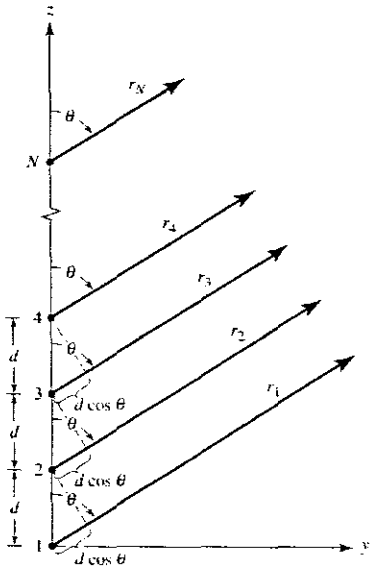

Figure A.2: Geometry of an *N*-element array along the z-axis with far-field observation (Adapted from Balanis, 2005:293).

Equation (A-13) can then be written as

$$AF = \frac{(e^{jN\psi} - 1)}{(e^{j\psi} - 1)} = e^{j[(N-1)/2]\psi}\left[\frac{e^{j(N/2)\psi} - e^{-j(N/2)\psi}}{e^{j(1/2)\psi} - e^{-j(1/2)\psi}}\right]$$
$$= e^{j[(N-1)/2]\psi}\left[\frac{\sin(\frac{N}{2}\psi)}{\sin(\frac{1}{2}\psi)}\right] \qquad \textbf{(A-14)}$$

Taking the physical centre of the array as the reference point, then equation (A-14) can be written as

$$AF = \left[\frac{\sin(\frac{N}{2}\psi)}{\sin(\frac{1}{2}\psi)}\right]. \qquad \textbf{(A-15a)}$$

Equation (A-15a) can be approximated for small values of ψ as

$$AF \approx \left[\frac{\sin(\frac{N}{2}\psi)}{\frac{\psi}{2}}\right]. \qquad \textbf{(A-15b)}$$

Sometimes it is convenient to write the AF as in equation (A-15a) and equation (A-15b) in their normalised forms respectively as

$$(AF)_n = \frac{1}{N}\left[\frac{\sin(\frac{N}{2}\psi)}{\sin(\frac{1}{2}\psi)}\right]. \qquad \textbf{(A-16a)}$$

$$(AF)_n \approx \left[\frac{\sin(\frac{N}{2}\psi)}{\frac{N}{2}\psi}\right]. \qquad \textbf{(A-16b)}$$

Through investigation it can be proven that the maximum of the first minor lobe amounts to 13.46 dB below the maximum at the major lobe.

A.1.2.1Broadside array

The direction of the maximum peak of the radiation beam can be adopted for classifying the type of array. The first being a broadside array with the maximum radiation directed broadside to the axis of the array. The broadside direction refers to $\theta_0 = 90°$ therefore substituting this in equation (A-17) gives the relative phase (progressive phase) between elements as

$$\psi = kd\cos\theta + \beta\big|_{\theta=90°} = \beta = 0°. \qquad \textbf{(A-17)}$$

This is the required phase to have the maximum of the AF directed toward broadside.

A.1.2.2Ordinary End-Fire array

When the maximum radiation takes place along the axis of the array it is known as an Ordinary End-fire array. The maximum can be directed towards the $\theta_0 = 0°$ or $\theta_0 = 180°$. The resulting relative phase for the $\theta_0 = 0°$, is determined as

$$\psi = kd\cos\theta + \beta\big|_{\theta=0°} = kd + \beta = 0° \Rightarrow \beta = -kd \qquad \textbf{(A-18)}$$

and to point the beam towards the $\theta_0 = 180°$ direction gives a relative phase of

$$\psi = kd\cos\theta + \beta\big|_{\theta=180^\circ} = -kd + \beta = 0^\circ \Rightarrow \beta = kd\,. \qquad \textbf{(A-19)}$$

A.1.2.3Phased (Scanning) array

Controlling the phase excitation between the elements results in an array with a maximum beam that can be oriented in any direction and is termed a phased or scanning array. The procedure is similar to the end-fire array for finding the relative excitation phase for each element. Thus for a maximum to occur between θ_0 ($0^\circ \leq \theta_0 \leq 180^\circ$), therefore solving the relative phase in equation (A-20), gives the relative phase as

$$\psi = kd\cos\theta + \beta\big|_{\theta=\theta_0} = kd\cos\theta_0 + \beta = 0^\circ \Rightarrow \beta = -kd\cos\theta_0\,. \qquad \textbf{(A-20)}$$

In practice the excitation phase in a phased array antenna is altered by electronically adjusting the phase through the use of electronic phase shifters.

A.1.3 N-element linear array with non-uniform amplitude and uniform spacing

The SLLs achieved utilising linear arrays with uniform amplitude distributions does not meet the stringent sidelobe requirements which are key in present day radar and communication systems. It is thus needed to taper the excitation currents of the elements on the edges of the array. This action produces an array which is fired or excited hard through the centre elements and less through the edge elements. The amount of energy applied to the elements in a linear array has been studied and established several years ago and standard excitation coefficients or amplitude distributions exist. The two most known non-uniform amplitude distributions utilised to achieve low sidelobes include the Binomial, Dolph-Tschebyscheff and Taylor distributions.

The *AF* of a linear array with non-uniform amplitude excitation can be found by assuming isotropic elements positioned along the z-axis as in the uniform case. Two terms exist then for the *AF* corresponding to two possible configurations for an even number of elements $2M$ and an odd number of elements $2M+1$ given by

$$(AF)_{2M}(even) = \sum_{n=1}^{M} a_n \cos[(2n-1)u] \quad \textbf{(A-21a)}$$

$$(AF)_{2M+1}(odd) = \sum_{n=1}^{M+1} a_n \cos[2(n-1)u] \quad \textbf{(A-21b)}$$

where M is an integer, $u = \frac{\pi d}{\lambda}\cos\theta$, d is the element spacing and a_n the excitation coefficients of the array.

A.1.3.1Binomial array

The excitation coefficients for a Binomial distribution is given by writing the function $(1+x)^{m-1}$ in a series using the binomial expansion given as

$$(1+x)^{m-1} = 1 + (m-1)x + \frac{(m-1)(m-2)}{2!}x^2 + \frac{(m-1)(m-2)(m-3)}{3!}x^3 + \ldots \quad \textbf{(A-22)}$$

Therefore for an array with M-elements, equation (A-22) resides to a Pascal's triangle with the coefficients of the expansion corresponding to the relative amplitudes of the elements in the array. Another method to low sidelobes in linear arrays is to have a Dolph-Tschebyscheff distribution.

A.1.3.2Dolph-Tschebyscheff array

Relating the excitation coefficients to the Tschebyscheff polynomials results in a radiation pattern with uniform sidelobes of a desired value. This distribution is a compromise between the Uniform and Binomial array in the sense that a Tschebyscheff array with no sidelobes amounts to a Binomial design. As seen in equation (A-21a) and equation (A-21b) it is perceptible that for an even or odd element array with identical amplitudes, the AF is simply the summation of cosine terms. These cosine terms is written as a series of cosine functions and is related to the Tschebyscheff polynomial $T_m(z)$. Figure A.5 illustrates the first six Tschebyscheff polynomials

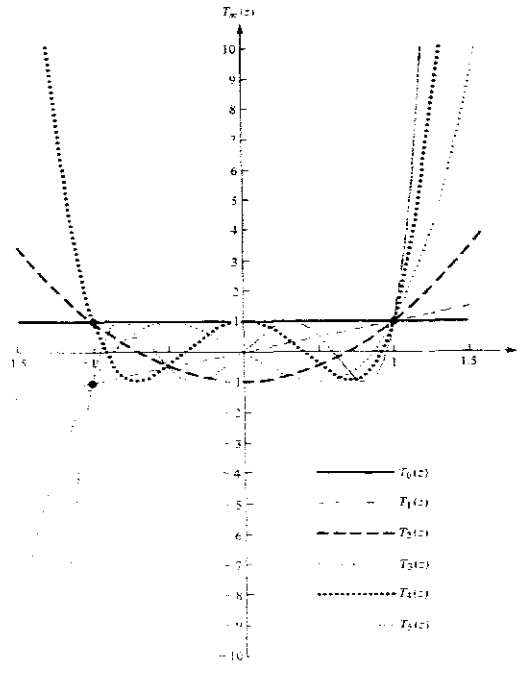

Figure A.5: First six Tschebyscheff polynomials. (Adapted from Balanis, 2005:334)

The cosine functions are valid for the condition $-1 \le z \le +1$. Since $|\cos(mu)| \le 1$, therefore each Tschebyscheff polynomial is $|Tm(z)| \le 1$ for $-1 \le z \le +1$. The Tschebyscheff polynomials are related to the hyperbolic cosine functions for $|z| > 1$. The recursion formula for finding the Tschebyscheff polynomials is given as

$$T_m(z) = 2(z)T_{m-1}(z) - T_{m-2}(z). \qquad \textbf{(A-23)}$$

Each polynomial can be computed using

$$T_m(z) = \cos\left[m\cos^{-1}(z)\right] \quad -1 \le z \le +1 \qquad \textbf{(A-24)}$$

$$T_m(z) = \cosh\left[m\cosh^{-1}(z)\right] \quad z < -1, z > +1 \qquad \textbf{(A-25)}$$

The polynomials have the following properties:

- All passes through the point (1, 1).
- For $-1 \le z \le +1$ the values is within -1 to +1.
- All roots occur within $-1 \le z \le +1$ and maxima and minima are +1 and −1 respectively

The design procedures and examples as well as further information regarding these types of arrays are elaborated in the literature by Skolnik (1970), Balanis (2005) and Volakis (2007) and will not be discussed here. The following observations are of importance regarding non-uniform arrays and when deciding on the type of aperture distribution for a particular application:

- Uniform arrays yield the smallest HPBW, followed by Tschebyscheff and Binomial arrays.
- Binomial arrays possess the smallest SLLs followed by Tschebyscheff and uniform arrays

The designer is left with a trade off between SLL and beamwidth and it has been proven analytically that for a given SLL the Dolph-Tschebyscheff yields the narrowest FNBW. Therefore the Dolph-Tschebyscheff design results in the smallest SLL for a given FNBW. It is this property which resulted in the design of a –25 dB Dolph-Tschebyscheff array to achieve the smallest SLL for the narrowest HPBW possible favoured in radar applications. Other distributions exist with their own advantages and trade-offs. These include Taylor and Villeneuve distributions, to mention only two. All the analyses done on arrays are based on an isotropic radiator as elements, however, in the real world antenna array elements need to meet certain requirements such as small size, radiation pattern, polarisation and inexpensive materials and construction.